

UC San Diego

UC San Diego Previously Published Works

Title

Dipicolinic Acid Derivatives as Inhibitors of New Delhi Metallo- β -lactamase-1

Permalink

<https://escholarship.org/uc/item/3bf0j2rq>

Journal

Journal of Medicinal Chemistry, 60(17)

ISSN

0022-2623

Authors

Chen, Allie Y
Thomas, Pei W
Stewart, Alesha C
[et al.](#)

Publication Date

2017-09-14

DOI

10.1021/acs.jmedchem.7b00407

Peer reviewed



Published in final edited form as:

J Med Chem. 2017 September 14; 60(17): 7267–7283. doi:10.1021/acs.jmedchem.7b00407.

Dipicolinic Acid Derivatives as Inhibitors of New Delhi Metallo- β -lactamase-1

Allie Y. Chen¹, Pei W. Thomas², Alesha C. Stewart², Alexander Bergstrom³, Zishuo Cheng³, Callie Miller³, Christopher R. Bethel⁴, Steven H. Marshall⁴, Cy V. Credille¹, Christopher L. Riley⁵, Richard C. Page³, Robert A. Bonomo^{4,6,*}, Michael W. Crowder^{3,*}, David L. Tierney^{3,*}, Walter Fast^{2,*}, and Seth M. Cohen^{1,*}

¹Department of Chemistry and Biochemistry, University of California, San Diego, La Jolla, CA 92093, United States

²Division of Chemical Biology & Medicinal Chemistry, College of Pharmacy, University of Texas, Austin, TX 78712, United States

³Department of Chemistry and Biochemistry, Miami University, Oxford, OH 45056, United States

⁴Research Services, Louis Stokes Cleveland Department of Veterans Affairs Medical Center, Cleveland, OH 44106, United States

⁵Department of Molecular Biosciences, University of Texas, Austin, TX 78712, United States

⁶Departments of Medicine, Molecular Biology and Microbiology, Biochemistry, and Pharmacology, Case Western Reserve University, Cleveland, OH 44106, United States

Abstract

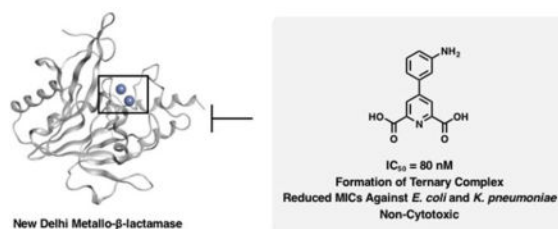
The efficacy of β -lactam antibiotics is threatened by the emergence and global spread of metallo- β -lactamase-(MBL) mediated resistance, specifically New Delhi-Metallo- β -lactamase-1 (NDM-1). Utilizing fragment-based drug discovery (FBDD), a new class of inhibitors for NDM-1 and two related β -lactamases, IMP-1 and VIM-2, was identified. Based on 2,6-dipicolinic acid (DPA), several libraries were synthesized for structure-activity relationship (SAR) analysis. Inhibitor **36** (IC₅₀ = 80 nM) was identified to be highly selective for MBLs when compared to other Zn(II) metalloenzymes. While DPA displayed a propensity to chelate metal ions from NDM-1, **36** formed a stable NDM-1:Zn(II):inhibitor ternary complex, as demonstrated by ¹H NMR, electron paramagnetic resonance (EPR) spectroscopy, equilibrium dialysis, intrinsic tryptophan fluorescence emission, and UV-Vis spectroscopy. When co-administered with **36** (at concentrations non-toxic to mammalian cells), the minimum inhibitory concentration (MIC) of

*To whom correspondence should be addressed: Seth M. Cohen: scohen@ucsd.edu. Telephone: (858) 822-5596. Walter Fast: walt.fast@austin.utexas.edu. Telephone: (512) 232-4000. Michael W. Crowder: crowdemw@miamioh.edu. Telephone: (513) 529-2813. David L. Tierney: dtierney@miamioh.edu. Telephone: (513) 529-8234. Robert A. Bonomo: robert.bonomo@va.gov. Telephone: (216).791.3800.

Supporting Information. Z' factor plots, primary screening hits, steady state kinetic parameters for fluorocillin, IC₅₀ determination, IC₅₀ variation with ZnSO₄, molecular modeling, ¹H NMR spectroscopy controls, cytotoxicity assay, cell imaging, molecular formula strings. Crystallographic data on compound **41** can be obtained free of charge from Cambridge Crystallographic Data Centre at www.ccdc.cam.ac.uk/data_request/cif (CCDC 1550829). Supporting Information is available free of charge on the ACS Publications website.

imipenem against clinical isolates of *Escherichia coli* and *Klebsiella pneumoniae* harboring NDM-1 were reduced to susceptible levels.

Graphical Abstract



Antibiotic-resistant in pathogenic bacteria has become a critical public health threat.¹ A major mechanism of antibiotic resistance is microbial degradation of drugs by enzymes such as β -lactamases. Three classes of β -lactamases (A, C, and D)² utilize an active-site serine in covalent mechanisms that can be targeted by β -lactamase inhibitors co-formulated with β -lactam drugs. In contrast, class B consists of metallo- β -lactamases (MBLs) that utilize one or two active site Zn(II) ion(s) to catalyze the hydrolysis of the β -lactam ring.³ MBLs have a broad substrate scope that enables hydrolysis of bicyclic β -lactams, but due to MBLs employing a different reaction mechanism, they evade the current β -lactamase inhibitors used in approved drug combinations. Thus, MBLs can confer resistance to the entire category of β -lactam drugs, except monobactams.^{4,5} MBLs with the greatest clinical impact are found in the B1 subfamily, with New Delhi Metallo- β -Lactamase-1 (NDM-1), Verona Integrin-encoded MBL (VIM-2), and Imipenemase (IMP-1) serving as examples. Of these, NDM-1 represents the most troubling development due to its carriage on easily transmissible plasmids and the emergence of community-acquired infections in addition to nosocomial infections typically found carrying other MBLs.⁵⁻⁸

Despite ongoing efforts to identify NDM-1 inhibitors, approved drugs to counter its activity are not yet available. Development of NDM-1 inhibitors has been slow due to a number of factors, including a shallow, relatively featureless active site that has is difficult to target,⁹ concerns about a lack of inhibitor selectivity leading to in vivo metal stripping or off-target inhibitory activity,¹⁰⁻¹² and a lack of novel scaffolds that selectively target the active site. Three examples of NDM-1 inhibitors are presented in Table 1. The hypertension drug L-captopril¹³ represents the repurposing of this sulfhydryl-containing inhibitor.¹⁴⁻¹⁶ Both D- and L-captopril have been reported as inhibitors of NDM-1, with IC_{50} values of $\sim 8 \mu\text{M}$ and $\sim 200 \mu\text{M}$, respectively.^{13,14} A crystal structure of L-captopril bound to NDM-1 reveals the thiolate bound in a β -bridging fashion between the Zn(II) ions, displacing the catalytic hydroxide anion.¹³ Although a crystal structure of the more potent D-captopril bound to NDM-1 is not available, analysis shows that the thiol of each isomer likely interacts with the dinuclear Zn(II) center in a similar manner,^{13,17} and the carboxylate of the D-isomer may mimic the carboxylate conserved in most β -lactam substrates. However, adverse effects associated with thiol-containing compounds may present a therapeutic liability for captopril and its derivatives.^{18,19}

A second example of a NDM-1 inhibitor is aspergillomarasmine A (AMA), a fungal natural product identified through cell-based screening (IC_{50} value = 4.0 μ M).¹² Combination therapy of AMA with meropenem was effective in microbial culture and in mice infected with a lethal dose of NDM-1-positive *K. pneumoniae*. However, the structural similarity of AMA to metal chelators such as ethylenediaminetetraacetic acid (EDTA) raises the possibility of off-target effects. This is consistent with the finding that AMA inhibits NDM-1 through a metal-chelation/stripping mechanism.¹²

A third example is the cyclic boronate shown in Table 1. This and related compounds exhibit excellent activity against NDM-1 (IC_{50} = 4 nM) as well as VIM-2, IMP-1, and *Bacillus cereus* MBL (BcII).²⁰ Investigation of these cyclic boronates as inhibitors of B1 MBLs reveal a binding mode that mimics substrate binding, including the formation of a tetrahedral complex. The similarity of these inhibitors to a β -lactam tetrahedral intermediate transition state may underlie the impressive activity of these compounds. More comprehensive reviews of MBL inhibitors are provided elsewhere,^{21–23} but these three examples illustrate some successful strategies and pitfalls in developing effective inhibitors for this class of enzymes.

Herein, we report a fragment-based drug discovery (FBDD)²⁴ strategy for the design, synthesis, and evaluation of a novel class of NDM-1 inhibitors. A focused library of metal-binding pharmacophores (MBPs) enabled a systematic search of compounds that target the dinuclear Zn(II) site of B1 MBLs. SAR analysis and optimization of primary hit 2,6-dipicolinic acid (DPA) led to the discovery of **36** with an IC_{50} value of ~80 nM, putting it on par with the most potent NDM-1 inhibitors presently reported in the literature.²⁰ Compound **36** showed increase inhibition against IMP-1 and VIM-2 when compared to DPA, and no significant inhibition against several other Zn(II)-dependent metalloenzymes. The interaction of **36** with the active site of di-Zn(II) or di-Co(II) metalloforms of NDM-1 was characterized via ¹H NMR spectroscopy, electron paramagnetic resonance (EPR) spectroscopy, equilibrium dialysis, intrinsic tryptophan fluorescence quenching, and UV-Vis spectroscopy. As inhibition of the lead compound was improved, a metal ion stripping mechanism was replaced in favor of a ternary NDM-1:Zn(II):inhibitor complex mechanism of action. Microdilution broth studies performed with clinical *E. coli* and *K. pneumoniae* strains harboring *bla*_{NDM-1} reveal that co-administration with **36** significantly reduced the minimum inhibitory concentration (MIC) values of imipenem. Furthermore, no toxicity was observed for **36** against a mammalian cell culture.

Results and Discussion

Screening of MBP Library and Selection of DPA for Optimization

The extreme sequence diversity found within the family of MBL proteins complicates the design of a single compound to serve as an effective broad spectrum MBL inhibitor. Even within the B1 subclass of MBLs, which contains the most clinically relevant targets, sequence identity is low. Pairwise protein sequence alignments between all combinations of the three MBLs tested here (NDM-1, IMP-1, and VIM-2) have identities of approximately only 30%.^{9,25} This diversity is also present at the active site where very few residues are essential for catalysis due to a mechanism that relies mostly on substrate interactions with the di-Zn(II) site.⁹ However, this same property makes the di-Zn(II) active site an attractive

target for inhibition by MBPs. MBPs are small molecular fragments that are known to have the capacity to bind metal ions in the active site of metalloproteins. The Cohen laboratory has assembled a MBP library consisting of ~300 fragments and this focused library has been shown useful in the development of other metalloprotein inhibitors, including antibacterial virulence factors.²⁶⁻³¹ Here, we search for MBL inhibitors through a more systematic exploration of chemical space by screening the MBP library against three representative B1 MBLs (NDM-1, IMP-1, and VIM-2). Several MBPs were identified as attractive leads for MBL inhibitor development.

A 96-well plate, continuous assay was optimized for the hydrolysis of the colorimetric β -lactam substrate chromacef by NDM-1 (substrate concentration = $3 \times K_M$), IMP-1 (substrate concentration = K_M), and VIM-2 (substrate concentration = K_M). The substrate concentrations were kept close to K_M values to better detect competitive inhibitors, yet high enough to allow for maintenance of linear initial rates.³² The assays showed good discrimination between positive (enzyme added) and negative (enzyme omitted) samples, with Z' factors of 0.7, 0.7, and 0.8 for NDM-1, IMP-1, and VIM-2, respectively (Figure S1).³³ Each fragment in the MBP library was screened at a concentration of 50 μ M against each of the three MBL enzymes and the resulting percent inhibition was measured. The activity of MBPs ranged from 0 – 100% inhibition, with an average of ~27% inhibition for the entire library screened against all three enzymes. Using a cutoff of >60% inhibition, six compounds remained as hits (Figure 1). One primary hit, 1,10-phenanthroline, is a known metal stripping agent and was omitted. Another hit, 2-(pyridine-2-yl)-4,5-dihydrothiazole, was disregarded because mass spectrometry indicated the stock solution of the MBP had degraded (data not shown). The remaining four primary hits consisted of: 3-hydroxypyridine-2(1*H*)-thione, which shares some structural similarities to the known MBL inhibitor thiomaltol;³⁴ two 8-hydroxyquinoline compounds, shown to inhibit a different di-Zn(II) enzyme,³⁵ and 2,6-dipicolinic acid (DPA). DPA was selected as the initial scaffold for optimization because previous reports describe dicarboxylate compounds and 2-carboxypyridines as inhibitors of other MBLs.^{9,36} Furthermore, DPA bears resemblance to the core of a hydrolyzed cephalosporin, mimicking both the carboxylate formed upon β -lactam hydrolysis and the leaving group nitrogen. The inhibition of DPA was first determined via colorimetric assay to have an $IC_{50} = 520$ nM.

Design and Synthesis of DPA Derivatives

To augment the inherent affinity of DPA for the Zn(II) component of MBLs, we sought to design DPA-based inhibitors of NDM-1 that focus on increasing the binding interactions with protein residues surrounding the active-site Zn(II) ions. The active site of NDM-1 (Figure 2) includes a mobile β -hairpin loop, which moves over the Zn(II) ions and back to the original position in the millisecond timescale.³⁷ This β -hairpin loop likely plays a role in ligand binding and/or catalysis, in part by presenting a flexible hydrophobic surface as one wall of the active site. Flanking the di-Zn(II) active site are two sides of a shallow, relatively featureless hydrophobic channel. This channel has a few notable residues available as potential binding partners, Asn220, Gln123, and Lys211. Based on the structure of the coordination complex of DPA with free Zn(II),³⁸ we assumed a similar coordination at the active site of NDM-1 to guide inhibitor optimization. The design and synthesis of

subsequent sublibraries aimed to improve interactions with amino acid residues surrounding the di-Zn(II) site.

The first of three sublibraries contained compounds with substituents designed to extend into the hydrophobic channel, as well as determine the necessity of both carboxylate groups on the DPA fragment for inhibition. These substitutions were introduced through the conversion of one of the carboxylate groups of DPA to various amide substituents via standard peptide coupling procedures (Compounds **3–20**, Scheme 1). The carboxylic acids of DPA were first esterified to give the dimethyl ester derivative **1**, then hydrolyzed with KOH at 0 °C to obtain the monomethyl ester **2** product. Coupling **2** with primary amines by 1-ethyl-3-(3-dimethylaminopropyl)carbodiimide (EDC) and hydroxybenzotriazole (HOBT) afford the desired amide derivatives. Finally, hydrolysis of the methyl ester in 1M NaOH/THF produced the mono-carboxylic acid DPA derivatives that comprise sublibrary 1 (**3–20**).

The second sublibrary (Compounds **22–30**) consisted of DPA derivatives with substituents at the 4-position of the pyridine ring connected through an amine linker (Scheme 2). This sublibrary was designed to determine what substituents could be tolerated in the active site pocket below the β -hairpin loop. Compounds **22–30** were synthesized starting from dimethyl 4-chloropyridine-2,6-dicarboxylate followed by saponification in a 1 M NaOH/THF solution to afford **21**. Next, **21** was heated using a microwave reactor in the presence of the corresponding amine to generate compounds **22–30**.

Lastly, the third sublibrary (Compounds **33–47**) also contained DPA derivatives with substituents at the 4-position, but incorporated a series of substituted aryl substituents to enhance possible hydrophobic interactions at the base of the β -hairpin loop, and included substitutions to make possible hydrogen bonding interactions with nearby residue side chains (e.g., Asn220, Gln123). In this sublibrary, instead of an amine linker, the aryl substituents are attached through a direct carbon-carbon bond formed via Pd-catalyzed Suzuki cross-coupling (Scheme 3). 4-Hydroxypyridine-2,6-dicarboxylic acid was esterified to **31** by heating to reflux in MeOH with catalytic H₂SO₄. Next, **31** was converted into the bromide derivative **32** using tetrabutylammonium bromide (TBAB) and phosphorus pentoxide (P₄O₁₀). Compounds **33–47** were then synthesized via Suzuki cross-coupling procedures utilizing Pd(PPh₃)₄ and K₃PO₄/CH₃CO₂K, with the final compounds obtained by saponification with 1 M NaOH/THF.

In Vitro Activity of DPA Derivatives as NDM-1 Inhibitors

An initial ranking of NDM-1 inhibition by DPA derivatives in sublibraries 1–3 was first completed by determining the IC₅₀ values using the colorimetric substrate chromacef. Chromacef, at a concentration of $3 \times K_M$, allowed for linear hydrolysis rates over the assay duration. A secondary assay, using the fluorescent substrate fluorocillin,^{16,39} was then used to verify ranking of the most potent compounds (sublibrary 3). By using a concentration less than K_M (Supporting Information), the fluorescent substrate allowed for increased signal response, a longer linear portion of the kinetic assay, and minimized substrate perturbation of IC₅₀ values for competitive inhibitors. Addition of a fluorescence-based assay also provides an orthogonal method to verify inhibition. False positives in the screen arising from

compounds with absorbance at wavelengths similar to the product detected in the absorbance-based assay would not interfere with the excitation or emission wavelengths used in the fluorescence-based assay. IC_{50} values determined using either substrate give similar relative rankings of potency, but are of different absolute magnitudes due to differing assay conditions (most significantly substrate concentration relative to K_M values).³² A summary of the inhibition data is provided in Table 2A and 2B.

Utilizing a colorimetric assay, it was found that most of the compounds in sublibrary 1 (**3–20**) showed 100-fold loss in activity when compared to the unsubstituted DPA ($IC_{50} = 520$ nM). This indicates that both carboxylate groups on DPA are required for inhibition. Both large (**8**) and small (**15**) substitutions were detrimental; however, substituents that reintroduce a potential metal coordinating ligand (**12–14**) retained some activity. DPA derivatized with D-valine (**14**), in comparison with **13** and **16** suggests that a carboxylate at this position drives activity, and that bulky hydrophobic substitutions can also improve inhibition, albeit to a lesser degree. Based on this SAR, both carboxylates of the DPA scaffold were retained in the design of subsequent sublibraries.

Compounds in sublibrary 2 (**21–30**) showed a modest loss in inhibition (7- to 26-fold) relative to DPA, with a small dimethylamine substituent (**22**) causing the most significant loss. Addition of a hydrophobic aryl group to the nitrogen linker (as in compound **23**) significantly rescued activity and resulted in the most potent inhibitor in this series ($IC_{50} = 3.4$ μ M). Extending the length of the linker (**23** vs. **24** or **25**) reduced activity. Substitution of the aryl ring (**26–28**) or replacement with different heterocycles (**29–30**) did not result in any significant improvement. These results suggest that substitution at the 4-position by an amine linkage is not favorable (even relative to unsubstituted DPA), but addition of hydrophobic substituents can rescue activity. These results are consistent with the hypothesis that substitution at this position can lead to interactions with the hydrophobic surface presented by the β -hairpin loop adjacent to the active site (Figure 2). Therefore, the aryl substituent was kept in the design of the third sublibrary, but a different linkage was utilized.

In contrast to the previous two sublibraries, compounds in sublibrary 3 (**33–47**) showed inhibition of NDM-1 that is on the same order of magnitude as DPA, and in some cases, significantly better. Examination of the fluorescent assay results reveal that DPA with aryl groups containing ortho-substituents (**38–39**) showed similar or improved inhibition relative to DPA ($IC_{50} = 410$ nM). In general, those with para-substituents (**40–43**) showed modest changes in inhibition. The same general trend is seen with meta-substitutions (**34–35**, **37**, **44–47**), except for compound **36**. Compound **36** stood out in sublibrary 3, with an IC_{50} value of 80 ± 2 nM (Figure S2). This compound represents a 4-fold improvement in inhibition compared to DPA, and achieves one of the lowest IC_{50} values for NDM-1 reported to date. Comparison of **36** with **42** suggests that the increase in inhibition is not likely due to the electron donating effects of **36** on metal binding, as a greater effect would be expected from the para-substituted compound. The substitution of a methoxy (**34**), alcohol (**35**), or dimethyl amine (**37**) group at the same position shows a loss in activity, suggesting that specific interactions (possibly by hydrogen bond donation) of **36** with the protein are responsible for the improved inhibition. It is proposed that aryl substituents directly linked to the 4-position of DPA augmented by meta-substituents are capable of specific protein

interactions, and represent an effective route for fragment growth. Notably, addition of exogenous Zn(II) in the assay buffer has little impact on the IC₅₀ value of **36**, suggesting a specific, direct interaction of **36** with amino acid residues in the active site of NDM-1. In contrast, exogenous Zn(II) in the assay buffer diminishes the inhibition activity of DPA against NDM-1, presumably due to sequestering of the excess Zn(II) by DPA (Figure S3).

In comparison with the most potent NDM-1 inhibitor currently reported, a diamino-substituted cyclic boronate²⁰ (Table 1, IC₅₀ = 4 nM), **36** is a smaller, achiral compound with a higher ligand efficiency (0.5 versus 0.4 kcal/mol/non-H atom).⁴⁰ Furthermore, a review profiling 3,200 antibacterial project compounds with whole cell activity found that active compounds against Gram-negative bacteria have an average of calculated log *D* (clogD pH 7.4) of <0.⁴¹ The clogD_{7.4} of **36** (-5.19 ~ -4.48) falls into the typical hydrophobic region of such antibacterial drugs. Structural determination of the ternary complex between **36** with NDM-1 is in progress and will be required to reveal the precise active site interactions, but molecular modeling suggests that placement of the DPA scaffold at the dinuclear Zn(II) active site may position the 4-aryl substituent near the hydrophobic base of the active-site β-hairpin loop, and situate the meta-substituent close to active site Asn220 (Figure S4). Molecular docking studies for metalloproteins are rather challenging, hence we consider the model here as a rough guide until more conclusive data on the binding of DPA and compound **36** are obtained.

Investigation of Inhibitor Selectivity

To determine the selectivity of **36** for MBLs, compound **36** was screened against two other B1 MBLs and a panel of other clinically relevant Zn(II)-dependent metalloenzymes. Despite the sequence diversity among B1 MBLs, the elaboration of DPA to **36** also resulted in enhancement of potency for inhibition of VIM-2 and IMP-1 (Table 3).

Inhibitor **36** was screened against a panel of Zn(II)-dependent metalloenzymes, including histone deacetylases (HDACs),⁴² matrix metalloproteinases (MMPs),⁴³ and carbonic anhydrases (CAs)⁴⁴ (Table 4). Screening protocols followed previously published procedures^{45,46} and values are reported as percent inhibition. At a concentration of 10 μM (significantly higher than the IC₅₀ value against NDM-1) compound **36** showed some inhibition against MMP-2 and MMP-12, but did not show inhibition against HDAC-1, HDAC-6, and human CAII. Testing **36** at higher concentrations (50 – 100 μM), resulted in some inhibition of these metalloenzymes; however, the inhibition values were <50% (data not shown). Based on the data obtained, compound **36** is between 100- and 1000-fold more selective for NDM-1 than for MMPs, between 500- and 1000-fold more selective for HDACs, and at least 500-fold more selective than for human CAII. Overall, **36** has strong activity against MBLs (NDM-1, IMP-1, VIM-2) and no significant inhibition of other Zn(II)-dependent metalloenzymes (at concentrations 10 μM, demonstrating the potential for **36** to be broad spectrum MBL inhibitor that does not exhibit off-target inhibition).

Mode of Inhibition

¹H NMR Spectroscopy—In previous work, we examined a series of M_{1,2}(II)-substituted analogs of NDM-1 (M_{1,2} = Co, Cd, Zn) by ¹H NMR.^{47,48} Comparing the CoCd and ZnCo

analogous to NDM-1, we assigned several resonances in the rich spectrum displayed by the CoCo enzyme (shown at the bottom of each panel in Figure 3). The solvent exchangeable resonances at 78, 73, and 65 ppm are ascribed to the three Co(II)-coordinated histidines at the Zn₁ site, while the peak at 107 ppm is assigned to the NH proton from His250 coordinated to Co(II) in the Zn₂ site. The sharp resonance at 47 ppm can be attributed to the β-CH₂ pair of Asp124, coordinated to Co(II) at the Zn₂ site, while the poorly resolved doublet near 170 ppm arises from β-CH₂ protons of the Co(II)-bound cysteine at the same site. In addition, several poorly resolved resonances attributed to secondary interactions between Co(II) in the Zn₂ site and distant residues in the substrate binding pocket, are seen in the range from +40 to -80 ppm.

With a paramagnet in both sites, and the ability to attribute many of the signals to either the Zn₁ or Zn₂ site, we used these signatures to examine the metal-binding properties of the individual inhibitors. CoCo-NDM-1 was titrated with increasing molar equivalents of DPA and **36**, along with a known chelator (EDTA) and a known competitive inhibitor (L-captopril)¹³ as controls. Each titration was compared to spectra from an aqueous solution of the inhibitor and Co(II), in the absence of protein (Figure S5). The NDM-1 titrations with L-captopril and EDTA gave results as expected, with L-captopril forming a ternary complex (Figure S6A) and EDTA (Figure S6B) indiscriminately removing metal. The titration with DPA (Figure 3A) shows evidence of metal removal at 1 equivalent, with the appearance of four very sharp, intense resonances at 102, 91, 37 and 30 ppm, consistent with the formation of the Co(DPA)_n adducts seen in control spectra. However, the rest of the spectrum is largely unaffected, suggesting that DPA indiscriminately removes both metal ions, and shows no changes that can be attributed to an NDM-1:Co(II):DPA ternary complex. Additional added DPA simply resulted in removal of both metal ions in the NDM-1 active site and further loss in signal intensity.

Titration of CoCo-NDM-1 with the DPA derivative **36** (Figure 3B) shows some evidence for metal ion removal; however, unlike DPA, **36** also shows evidence of a ternary complex formation. Addition of 1 equivalent of **36** led to a set of sharp resonances that indicate Co(**36**)_n formation (Figure S5). Although it is not possible to directly compare the intensity of these sharp lines to the broader lines of the Co(II) ligand protons, the relative intensity of these lines to those from Co(DPA)_n at 1 equivalent of added DPA is significantly lower. Meanwhile, at least two new resonances (red markers at ~125 and ~30 ppm) attributed with an NDM-1:Co(II):**36** ternary complex appears. At two equivalents of **36**, substantial metal removal is apparent, evidenced by loss of intensity particularly from the Zn₂ site ligands, suggesting **36** shows some preference for the formation of a ternary complex.

EPR Spectroscopy—To gain a better understanding of the ternary complex formed, we turned to EPR spectroscopy. As can be seen in Figure 4, the addition of 1 equivalent of DPA and **36** (similar to L-captopril, data not shown) led to minimal perturbation of the spectra, aside from minor modulation of the line shapes, when compared to the resting CoCo-NDM-1 spectra. The reason for small perturbations produced by L-captopril in the EPR spectra of NDM-1 is unknown, but consistent with similar previous findings.⁴⁹ This suggests the electronic structure of the Co(II) ions, and their physical structures, by extension, are largely unchanged. However, as shown in the inset, the addition of **36** led to a new feature

near 600 G, which has been seen in EPR studies of MBLs in the presence of substrates during turnover.⁵⁰ This feature, indicative of a more tightly coupled di-Co(II) site, is suggestive of an additional bridging species, arising from weak ferromagnetic coupling of the Co(II) ions. This can be more readily seen in the parallel mode spectra, which show a deep negative feature (~800 G) that appears on addition of 1 equivalent DPA and **36**. This data indicates not only the formation of a ternary complex, but bridging binding modes for both DPA and the synthesized inhibitor.

UV-Vis Spectroscopy—Previously, UV-vis spectroscopy has been used to probe Co(II) binding to NDM-1. The optical spectrum of CoCo-NDM-1 presented here (Figure 5A) is identical to that previously published, with ligand field transitions in the 500–700 nm region⁴⁸ from protein-bound high-spin Co(II) (the small absorbance at 420 nm has previously been attributed to the presence of Co(III)).⁵¹ Control spectra from buffered solutions of Co(II) in the presence of 3 eq of EDTA, captopril, DPA, or **36** showed minimal absorbance in the ligand field region (Figure S7), suggesting the presence or absence of the ligand field bands can serve as a marker for protein-bound Co(II). Titration of CoCo-NDM-1 with 1 eq of EDTA results in a small reduction of the intensities of all four ligand field transitions, suggesting removal of small amounts of Co(II). A second equivalent of EDTA results in complete loss of the ligand field transitions, indicating that EDTA fully removed Co(II) from the active site of NDM-1 (Figure 5A). Conversely, the titration of CoCo-NDM-1 with competitive inhibitor L-captopril (Figure 5B) results in a change in the shape of the ligand field bands, but no loss in intensity. While the inclusion of a second sulfur atom in the ligand set will surely complicate the interpretation of the captopril spectra, the retention of d-d band intensity strongly suggests the formation of an NDM-1:Co(II):captopril ternary complex. Titration of CoCo-NDM-1 with DPA was similar to that with EDTA, with the addition of the first equivalent of DPA resulting in a reduction in the ligand field intensity (Figure 5C), and a more dramatic reduction at 2 eq of DPA. While these data indicate that Co(II) is being removed from the active site, the retention of some ligand field intensity at 2 eq of DPA shows that DPA does not bind Co(II) as tightly as EDTA.⁵² Meanwhile, titration of CoCo-NDM-1 with **36** (Figure 5D) up to 2 eq shows minimal loss of d-d band intensity, suggesting minimal removal of the active site metal ion. The only perturbation produced by **36** is a strong charge-transfer transition at ca. 320 nm (an internal π - π^* transition of **36**) that alters the background associated with the ligand field region.

Equilibrium Dialysis—To be certain the mode of inhibition determined above is representative of the di-Zn(II) enzymes, equilibrium dialysis studies were conducted. Not surprisingly, the Zn(II) content of NDM-1 was significantly reduced when incubated with the metal chelator EDTA, while the Zn(II) content did not change upon incubation with L-captopril (Figure 6). Incubation of NDM-1 with DPA resulted in a significant loss in Zn(II) content, albeit not as much as EDTA at similar concentrations. Unlike DPA or EDTA, **36** behaves more like L-captopril. At low concentrations of **36**, incubation with NDM-1 resulted in no significant removal of Zn(II); only upon exposure to higher concentrations of these compounds (~24 μ M, about 240-fold greater than the IC₅₀ value) was 10–20% of the Zn(II) removed from NDM-1. This result further supports that the mode of inhibition

exhibited by **36** is through the formation of a NDM-1:Zn(II):inhibitor ternary complex, rather than metal stripping, even at micromolar concentrations.

Tryptophan Fluorescence—Previously, stopped-flow fluorescence studies were used to probe the kinetic mechanism of NDM-1.^{47,48} These studies revealed that the binding of substrate results in a rapid decrease in fluorescence, and as substrate is hydrolyzed and product is released, there is a rate-limiting return of fluorescence intensity. We attributed these fluorescence properties to Trp93, which is 5.7 Å from the Zn(II) binding site. As before, we utilized EDTA and L-captopril as controls to evaluate how a metal chelator versus a competitive inhibitor affects the fluorescence properties of NDM-1. Incubation of 2 μM NDM-1 with up to 32 μM EDTA resulted in <10% quenching of intrinsic tryptophan fluorescence (Figure 7A). Conversely, incubation of NDM-1 with up to 32 μM L-captopril resulted in a 10% increase in fluorescence, indicating a different binding mode for this compound. The increase in fluorescence is likely due to the interaction of C3 and C5 in L-captopril with Trp93.¹³ Incubation of NDM-1 with DPA resulted in a 20% quenching of tryptophan fluorescence emission (at 32 μM DPA where 20% of the Zn(II) was removed, Figure 6). In contrast, incubation of NDM-1 with **36** resulted in a 50–60% quenching of the intrinsic tryptophan fluorescence (Figure 7A). Due to the aromatic ring in **36**, we attribute the quenching of fluorescence to be due to the binding of these compounds to the metal center, resulting in a change in the fluorescence properties of Trp93. In support of this hypothesis, a control titration of L-tryptophan with EDTA, L-captopril, and **36** was performed. The titration of L-tryptophan with EDTA and L-captopril results in no change in the fluorescence emission of tryptophan, while titration with **36** results in a 50% reduction of fluorescence emission (Figure 7B). The results from fluorescence titrations are consistent with those from previous analysis, which indicate compound **36** is binding in the active site, forming a ternary NDM-1:Zn(II):inhibitor complex.

Microdilution Broth Minimum Inhibitory Concentrations (MICs)

Microdilution broth MICs were next performed on *E. coli* (Table 5) and *K. pneumoniae* (Table 6) clinical isolates expressing *bla*_{NDM-1}⁵³ using imipenem and compound **36**. The MICs of imipenem alone were 4 – 16 mg/L. Notably, the addition of compound **36** at 100 mg/L significantly lowered the imipenem MICs (0.5 – 1 mg/L). For all *E. coli* and *K. pneumoniae* strains, no effect on growth was observed with compound **36** alone, indicating a lack of toxicity at these concentrations. Even though standard CLSI guidelines have not yet been established for this imipenem:inhibitor combination, the reduction in MICs from 8 – 16 mg/L to 0.5 – 1 mg/L for the clinical strains would represent a reduction in MICs from the “resistant” to “susceptible” range. These results serve as an important proof of concept that these exploratory scaffolds are critical starting points for novel design strategies. Noteworthy, the β-lactam resistance profile in the selected strains is mediated by both extended-spectrum β-lactamases (ESBLs) (*bla*_{CTX-M-15}) and plasmid-mediated AmpCs (*bla*_{CMY-2}). A therapeutic combination of imipenem and **36** able to overcome the complex background of a metallo-β-lactamase (MBL), ESBL, and plasmid-mediated AmpC is notable. Furthermore, growth and morphology of cultured human HEK293 cells were also not adversely effected by **36** at concentrations relevant to the MIC studies (Figures S7, S8).

Conclusion

A FBDD strategy was applied to design potent inhibitors of the most clinically relevant MBLs. Previously, fragment-based approaches have been used for MBL inhibitor discovery.^{54–56} Here, the use of a small MBP fragment library enabled a systematic search for metal-directed inhibitors and identification of the scaffold DPA, which shares structural aspects of a hydrolyzed β -lactam product. Through the synthesis and screening of three sublibraries, compound **36** was identified as a broad spectrum, potent inhibitor of NDM-1, IMP-1 and VIM-2, arguably the most clinically important MBLs, with no significant inhibition of other Zn(II)-dependent metalloenzymes. A focus on screening MBP fragments to target the most conserved feature of MBLs, and the criteria of inhibiting three different MBLs in the primary screen, may have contributed to the success of this strategy in developing a potent pan-MBL inhibitor. Detailed spectroscopic characterization (¹H NMR, EPR, equilibrium dialysis, intrinsic tryptophan fluorescence emission, and UV-Vis) of the enzyme, inhibitor, metal:inhibitor, and the enzyme:metal:inhibitor ternary complexes reveal that an optimization of IC₅₀ values correlated with tighter formation of the ternary NDM-1:Zn(II):inhibitor complex. This work serves as a roadmap for converting a hit with metal-stripping tendencies into a potent metalloprotein-binding ligand. Microdilution broth MICs performed on a panel of highly-resistant clinical *E. coli* and *K. pneumoniae* strains harboring *bla*_{NDM-1} reveal that in all cases, **36** reduced imipenem MICs to a susceptible range and did not exhibit cytotoxicity against bacterial cells or human HEK293 cells. Compound **36** represents a new type of non-toxic, potent, pan-MBL inhibitor that is effective against clinical strains of carbapenem-resistant Enterobacteriaceae.

Experimental

Materials

All reagents and solvents were obtained from commercial sources and used without further purification. Nunc 96-well polystyrene clear flat bottom microplates, Corning black polypropylene round bottom 96-well microplates, Costar black polystyrene round bottom 96-well microplates, Costar clear polystyrene flat bottom 96-well microplates, 3-((3-cholamidopropyl) dimethylammonio)-1-propanesulfonate (CHAPS), 4-(2-hydroxyethyl)-1-piperazineethanesulfonic acid (HEPES), dimethyl sulfoxide (DMSO), and ethylenediaminetetraacetic acid (EDTA) and Fluorocillin green 495/525 β -lactamase substrate, soluble product, were purchased from Thermo Fisher Scientific Inc. (Fair Lawn, NJ). Chromacef was a generous gift from Dr. Larry Sutton (Benedictine College, Atchison, KS).⁵⁷ ([1,1'-Biphenyl]-4-ylsulfonyl)-D-phenylalanine (NSA) was prepared by literature methods.⁵⁸ All other reagents were purchased from Sigma-Aldrich Inc. (St. Louis, MO). High-throughput screening and chromacef assays were performed on a Perkin Elmer Victor 3V 1420 Multilabel Counter plate reader. Fluorescent assays were performed on a PerkinElmer Victor ³V fluorescent plate reader. Inhibitor selectivity absorbance and fluorescence assays were performed using a BioTek Synergy HT microplate reader. Microwave reactions were performed in 10 mL microwave vials using a CEM Discover S reactor. Column chromatography was performed using a Teledyne ISCO CombiFlash Rf system with prepacked silica cartridges. All ¹H NMR spectra were recorded at ambient

temperature using a 400 Varian Mercury FT-NMR instrument located in the Department of Chemistry and Biochemistry at the University of California, San Diego. Low Resolution (LR) mass spectrometry data were obtained from the University of California San Diego Chemistry and Biochemistry Mass Spectrometry Facility (MMSF). The purity of all compounds used in the assays were determined to be 95% by ^1H NMR spectroscopy and high performance liquid chromatography (HPLC).

Synthetic Procedures and Compound Characterization

Dimethyl pyridine-2,6-dicarboxylate (1)—Dipicolinic acid (1 g, 5.98 mmol) was dissolved in MeOH (1 L) and concentrated H_2SO_4 (0.5 mL) was added dropwise to the solution. The reaction mixture was heated to reflux for 24 h and monitored via TLC. Once the reaction was completed by TLC, the solvent was removed by evaporation in vacuo to afford **1** as a white crystalline solid in 100% yield (1.16 g, 5.96 mmol). No further purification was needed. ^1H NMR (400 MHz, DMSO- d_6): δ 8.26–8.13 (m, 3H), 3.90 (s, 6H). ESI-MS(+) calculated for $[\text{C}_9\text{H}_{10}\text{NO}_4]^+$ m/z 196.06, found m/z 196.09 $[\text{M}+\text{H}]^+$.

6-(Methoxycarbonyl)picolinic acid (2)—Dimethyl pyridine-2,6-dicarboxylate (1.9 g, 9.92 mmol) was dissolved in MeOH (75 mL) and cooled to 0°C via ice bath. Potassium hydroxide pellets (557 mg, 9.92 mmol) were added to the solution portion-wise and stirred at 0°C for an additional 4 h. Once the reaction was complete by TLC, the MeOH was removed by evaporation in vacuo. The white salt was washed with copious amounts of EtOAc to remove any remaining starting material. The salt was then dissolved in water (25 mL) and solution was acidified with 4M HCl to pH 2. The aqueous solution was extracted with chloroform (25 mL \times 3) and the combined organic layers were dried over MgSO_4 . MgSO_4 was removed by vacuum filtration and the organic layer was dried by evaporation in vacuo to afford **2** as a white powder in 81% yield (1.45 g, 8.00 mmol). ^1H NMR (400 MHz, DMSO- d_6): δ 8.23–8.14 (m, 3H), 3.90 (s, 3H). ESI-MS(–) calculated for $[\text{C}_8\text{H}_6\text{NO}_4]^-$ m/z 180.03, found m/z 180.09 $[\text{M}-\text{H}]^-$.

General Procedure for Compounds 3–20

6-(Methoxycarbonyl)picolinic acid (200 mg, 1.10 mmol), 1-ethyl-3-(3-dimethylaminopropyl)carbodiimide (EDC, 1.1 equivalents) and hydroxybenzotriazole (HOBT, 1.1 equivalents) were dissolved in dry DMF (10 mL) and the reaction mixture was stirred at room temperature for 30 min. The corresponding amine (1.1 equivalents) was then added and the reaction mixture and allowed to react at room temperature overnight. DMF was dried by evaporation in vacuo, and the reaction was taken up in EtOAc (10 mL), and extracted with copious amounts of saturated NaHCO_3 (10 mL \times 3). The organic layer was dried by evaporation in vacuo and purified by EtOAc and hexane column chromatography. Hydrolysis was then performed by stirring the product in a solution of 1M NaOH (4 mL) and THF (1 mL) at room temperature. Once the hydrolysis was complete by TLC, the solution was acidified with 4M HCl to pH 4 and the precipitate was collected via vacuum filtration.

6-(Phenylcarbamoyl)picolinic acid (3)—Yield: 85% (227 mg, 0.937 mmol). ^1H NMR (400 MHz, MeOD- d_4): δ 8.45 (d, $J=7.6$ Hz, 1H), 8.36 (d, $J=6.8$ Hz, 1H), 8.21 (m, 1H), 7.86

(d, $J=7.6$ Hz, 2H), 7.34 (t, $J=7.6$ Hz, 2H), 7.17 (t, $J=7.2$ Hz, 1H). ESI-MS(–) calculated for $[C_{13}H_9N_2O_3]^-$ m/z 241.06, found m/z 241.03 [M-H][–].

6-(Benzylcarbamoyl)picolinic acid (4)—Yield: 87% (185 mg, 0.722 mmol). ¹H NMR (400 MHz, MeOD-*d*₄): δ 8.34 (d, $J=7.2$ Hz, 1H), 8.30 (d, $J=7.2$ Hz, 1H), 8.15 (m, 1H), 7.38-7.23 (m, 5H), 4.63 (s, 2H). ESI-MS(–) calculated for $[C_{14}H_{11}N_2O_3]^-$ m/z 255.08, found m/z 255.23 [M-H][–].

6-(Phenethylcarbamoyl)picolinic acid (5)—Yield: 77% (231 mg, 0.853 mmol). ¹H NMR (400 MHz, MeOD-*d*₄): δ 8.31-8.29 (m, 2H), 8.15 (m, 1H), 7.27-7.26 (br s, 4H), 7.19 (t, $J=4$ Hz, 1H), 3.66 (t, $J=7.6$ Hz, 2H), 2.95 (t, $J=7.6$ Hz, 2H). ESI-MS(–) calculated for $[C_{15}H_{13}N_2O_3]^-$ m/z 269.09, found m/z 269.13 [M-H][–].

6-((4-Methoxyphenyl)carbamoyl)picolinic acid (6)—Yield: 79% (237 mg, 0.871 mmol). ¹H NMR (400 MHz, MeOD-*d*₄): δ 8.41 (d, $J=8$ Hz, 1H), 8.33 (d, $J=7.6$ Hz, 1H), 8.19 (m, 1H), 7.75 (d, $J=8.8$ Hz, 2H), 6.94 (d, $J=8.8$ Hz, 2H), 3.80 (s, 3H). ESI-MS(–) calculated for $[C_{14}H_{11}N_2O_4]^-$ m/z 271.07, found m/z 271.17 [M-H][–].

6-((4-Methoxybenzyl)carbamoyl)picolinic acid (7)—Yield: 81% (255 mg, 0.891 mmol). ¹H NMR (400 MHz, MeOD-*d*₄): δ 8.34 (d, $J=8$ Hz, 1H), 8.30 (d, $J=7.6$ Hz, 1H), 8.16 (m, 1H), 7.30 (d, $J=7.6$ Hz, 2H), 6.87 (d, $J=8$ Hz, 2H), 4.55 (s, 2H), 3.76 (s, 3H). ESI-MS(–) calculated for $[C_{15}H_{13}N_2O_4]^-$ m/z 285.08, found m/z 285.16 [M-H][–].

6-((Benzo[d][1,3]dioxol-5-ylmethyl)carbamoyl)picolinic acid (8)—Yield: 35% (116 mg, 0.386 mmol). ¹H NMR (400 MHz, MeOD-*d*₄): δ 8.33 (d, $J=15.2$ Hz, 1H), 8.31 (d, $J=14.8$ Hz, 1H), 8.16 (m, 1H), 6.88-6.75 (m, 3H), 5.91 (s, 2H), 4.53 (s, 2H). ESI-MS(–) calculated for $[C_{15}H_{11}N_2O_5]^-$ m/z 299.07, found m/z 299.04 [M-H][–].

6-((Furan-2-ylmethyl)carbamoyl)picolinic acid (9)—Yield: 79% (216 mg, 0.877 mmol). ¹H NMR (400 MHz, MeOD-*d*₄): δ 8.34-8.29 (m, 2H), 8.16 (m, 1H), 7.44 (s, 1H), 6.36-6.34 (m, 2H), 4.62 (s, 2H). ESI-MS(–) calculated for $[C_{12}H_9N_2O_4]^-$ m/z 245.06, found m/z 245.20 [M-H][–].

6-((Thiophen-2-ylmethyl)carbamoyl)picolinic acid (10)—Yield: 77% (223 mg, 0.850 mmol). ¹H NMR (400 MHz, MeOD-*d*₄): δ 8.34 (d, $J=7.6$ Hz, 1H), 8.30 (d, $J=7.6$ Hz, 1H), 8.16 (m, 1H), 7.29 (d, $J=4.8$ Hz, 1H), 7.08 (s, 1H), 6.96-6.94 (m, 1H), 4.79 (s, 2H). ESI-MS(–) calculated for $[C_{12}H_9N_2O_3S]^-$ m/z 261.03, found m/z 261.18 [M-H][–].

6-((2-(Thiophen-2-yl)ethyl)carbamoyl)picolinic acid (11)—Yield: 78% (231 mg, 0.836 mmol). ¹H NMR (400 MHz, MeOD-*d*₄): δ 8.31-8.29 (m, 2H), 8.15 (m, 1H), 7.19-7.18 (m, 1H), 6.91 (br s, 2H), 3.69 (t, $J=7.2$ Hz, 2H), 3.18 (t, $J=7.2$ Hz, 2H). ESI-MS(–) calculated for $[C_{13}H_{11}N_2O_3S]^-$ m/z 275.05, found m/z 275.07 [M-H][–].

6-((Thiazol-2-ylmethyl)carbamoyl)picolinic acid (12)—Yield: 34% (99 mg, 0.376 mmol). ¹H NMR (400 MHz, MeOD-*d*₄): δ 8.36-8.32 (m, 2H), 8.19 (m, 1H), 7.73 (s, 1H),

7.53 (s, 1H), 4.95 (s, 2H). ESI-MS(−) calculated for $[C_{11}H_8N_3O_3S]^-$ m/z 262.03, found m/z 261.98 $[M-H]^-$

6-((Carboxymethyl)carbamoyl)picolinic acid (13)—Yield: 57% (141 mg, 0.627 mmol). 1H NMR (400 MHz, MeOD- d_4): δ 8.33-8.31(m, 2H), 8.18 (m, 1H), 4.18 (s, 2H). ESI-MS(−) calculated for $[C_9H_7N_2O_5]^-$ m/z 223.04, found m/z 222.99 $[M-H]^-$, 245.13 $[M+Na-2H]^-$, 111.16 $[M-2H]^{2-}$.

(R)-6-((1-Carboxy-2-methylpropyl)carbamoyl)picolinic acid (14)—Yield: 62% (182 mg, 0.684 mmol). 1H NMR (400 MHz, MeOD- d_4): δ 8.34-8.32 (m, 2H), 8.17 (m, 1H), 4.53 (d, $J=6$ Hz, 1H), 3.30 (s, 1H), 1.07 (s, 6H). ESI-MS(−) calculated for $[C_{12}H_{13}N_2O_5]^-$ m/z 265.08, found m/z 265.04 $[M-H]^-$, 287.17 $[M+Na-2H]^-$, 303.16 $[M+K-2H]^-$.

6-(Isopropylcarbamoyl)picolinic acid (15)—Yield: 74% (170 mg, 0.816 mmol). 1H NMR (400 MHz, MeOD- d_4): δ 8.33-8.14 (m, 3H), 4.26-4.20 (m, 1H), 1.31 (s, 3H), 1.29 (s, 3H). ESI-MS(−) calculated for $[C_{10}H_{11}N_2O_3]^-$ m/z 207.08, found m/z 207.08 $[M-H]^-$.

6-(Isobutylcarbamoyl)picolinic acid (16)—Yield: 71% (130 mg, 0.585 mmol). 1H NMR (400 MHz, MeOD- d_4): δ 8.33-8.30 (m, 2H), 8.17 (m, 1H), 3.31-3.30 (m, 1H), 3.27 (s, 1H), 3.26 (s, 1H), 0.99 (s, 3H), 0.98 (s, 3H). ESI-MS(−) calculated for $[C_{11}H_{13}N_2O_3]^-$ m/z 223.11, found m/z 223.09 $[M+H]^-$.

6-(Cyclopentylcarbamoyl)picolinic acid (17)—Yield: 64% (168 mg, 0.175 mmol). 1H NMR (400 MHz, MeOD- d_4): δ 8.32-8.28 (m, 2H), 8.15 (m, 1H), 4.38-4.31 (m, 1H), 2.05 (br s, 2H), 1.82 (br s, 2H), 1.66 (br s, 4H). ESI-MS(−) calculated for $[C_{12}H_{13}N_2O_3]^-$ m/z 233.09, found m/z 233.12 $[M-H]^-$.

6-(Cyclohexylcarbamoyl)picolinic acid (18)—Yield: 64% (174 mg, 0.701 mmol). 1H NMR (400 MHz, MeOD- d_4): δ 8.33-8.29 (m, 2H), 8.17-8.13 (m, 1H), 3.98 (br s, 1H), 1.98 (br s, 2H), 1.84 (br s, 2H), 1.71 (d, $J=12$ Hz, 1H), 1.48-1.38 (m, 4H), 1.27 (br s, 1H). ESI-MS(−) calculated for $[C_{13}H_{15}N_2O_3]^-$ m/z 247.10, found m/z 247.11 $[M-H]^-$.

6-(((Tetrahydrofuran-2-yl)methyl)carbamoyl)picolinic acid (19)—Yield: 44% (121 mg, 0.484 mmol). 1H NMR (400 MHz, MeOD- d_4): δ 8.33-8.30 (m, 2H), 8.18-8.14 (m, 1H), 4.17-4.11 (m, 1H), 3.93-3.88(m, 1H), 3.79-3.74 (br s, 1H), 3.75-3.49 (m, 2H), 2.08-1.86 (m, 3H), 1.73-1.65 (m, 1H). ESI-MS(−) calculated for $[C_{12}H_{13}N_2O_4]^-$ m/z 249.09, found m/z 249.12 $[M-H]^-$.

6-(Piperidine-1-carbonyl)picolinic acid (20)—Yield: 58% (151 mg, 0.645 mmol). 1H NMR (400 MHz, MeOD- d_4): δ 8.21 (d, $J=8$ Hz, 1H), 8.12-8.08 (m, 1H), 7.74 (d, $J=7.6$ Hz, 1H), 3.74 (br s, 2H), 3.36 (t, $J=5.6$ Hz, 2H), 1.72 (br s, 4H), 1.60 (br s, 2H). ESI-MS(−) calculated for $[C_{12}H_{13}N_2O_3]^-$ m/z 233.09, found m/z 233.18 $[M-H]^-$.

4-Chloropyridine-2,6-dicarboxylic acid (21)—Dimethyl 4-chloropyridine-2,6-dicarboxylate (270 mg, 1.18 mmol) was dissolved in a solution of 1M NaOH (10 mL) and THF (1 mL). The reaction mixture was stirred at 70 °C for 3 h and monitored via TLC. Once

the reaction was complete by TLC, the THF was removed by evaporation in vacuo. The aqueous solution was washed with EtOAc (20 mL) to remove any remaining starting material. The aqueous phase was acidified with 4M HCl to pH 4 to obtain a yellow precipitate. The precipitate was collected via vacuum filtration and washed with copious amounts of water to afford **21** in 80% yield (190 mg, 0.94 mmol). ¹H NMR (400 MHz, DMSO-*d*₆): δ 8.14 (s, 2H). ESI-MS(–) calculated for [C₇H₃ClNO₄][–] *m/z* 199.97, found *m/z* 200.95 [M-H][–].

General Procedure for Compounds 22–30

In a microwave vessel, 4-chloropyridine-2,6-dicarboxylic acid (50 mg, 0.25 mmol, unless otherwise noted) and the corresponding amine (3 equivalents, unless otherwise noted) were suspended in water (2 mL). The reaction mixture was heated via microwave irradiation for 30 min at 160°C. The resulting solution was acidified with 4M HCl to pH 4, and the resulting precipitate was collected via vacuum filtration and washed with cold water.

4-(Dimethylamino)pyridine-2,6-dicarboxylic acid (22)—4-Chloropyridine-2,6-dicarboxylic acid (60 mg, 0.30 mmol) and dimethylamine (1.70 mL, 13.39 mmol). Yield: 64% (40 mg, 0.190 mmol). ¹H NMR (400 MHz, DMSO-*d*₆): δ 7.31 (s, 2H), 3.04 (s, 6H). ESI-MS(–) calculated for [C₉H₉N₂O₄][–] *m/z* 209.06, found *m/z* 208.95 [M-H][–].

4-(Phenylamino)pyridine-2,6-dicarboxylic acid (23)—4-Chloropyridine-2,6-dicarboxylic acid (70 mg, 0.35 mmol) and aniline (0.104 mL, 1.15 mmol). Yield: 59% (53 mg, 0.205 mmol). ¹H NMR (400 MHz, DMSO-*d*₆): δ 9.90 (s, 1H), 7.54 (s, 2H), 7.48-7.23 (m, 5H). ESI-MS(–) calculated for [C₁₃H₉N₂O₄][–] *m/z* 257.06, found 279.19 [M-H+Na][–].

4-(Benzylamino)pyridine-2,6-dicarboxylic acid (24)—4-Chloropyridine-2,6-dicarboxylic acid (54 mg, 0.27 mmol) and phenylmethanamine (100 mg, 0.94 mmol). Yield: 14% (10 mg, 0.037 mmol). ¹H NMR (400 MHz, DMSO-*d*₆): δ 8.92 (s, 1H), 7.35-7.03 (m, 7H), 4.56 (br s, 2H). ESI-MS(–) calculated for [C₁₄H₁₁N₂O₄][–] *m/z* 271.07, found *m/z* 270.98 [M-H][–].

4-(Phenethylamino)pyridine-2,6-dicarboxylic acid (25)—Yield: 80% (57 mg, 0.199 mmol). ¹H NMR (400 MHz, DMSO-*d*₆): δ 7.67 (t, *J*=5.6 Hz, 1H), 7.29-7.19 (m, 7H), 3.45 (q, *J*_F=6.4 Hz, *J*_Z=4 Hz, 2H), 2.85 (t, *J*=6.8 Hz, 2H). ESI-MS(–) calculated for [C₁₅H₁₃N₂O₄][–] *m/z* 285.09, found 307.21 [M-H+Na][–].

4-((4-Methoxyphenyl)amino)pyridine-2,6-dicarboxylic acid (26)—Yield: 35% (25 mg, 0.087 mmol). ¹H NMR (400 MHz, MeOD-*d*₄): δ 7.47 (s, 2H), 7.27 (d, *J*=8.8 Hz, 2H), 7.05 (d, *J*=8.8 Hz, 2H), 3.84 (s, 3H). ESI-MS(–) calculated for [C₁₄H₁₁N₂O₅][–] *m/z* 287.07, found, *m/z* 245.20 [M-H-CO₂][–].

4-((4-Methoxybenzyl)amino)pyridine-2,6-dicarboxylic acid (27)—Yield: 48% (36 mg, 0.119 mmol). ¹H NMR (400 MHz, DMSO-*d*₆): δ 8.44 (s, 1H), 7.27-6.90 (m, 6H), 4.42 (d, *J*=5.6 Hz, 2H), 2.72 (s, 3H). ESI-MS(–) calculated for [C₁₅H₁₃N₂O₅][–] *m/z* 301.08, found *m/z* 300.98 [M-H][–].

4-((Benzo[d][1,3]dioxol-5-ylmethyl)amino)pyridine-2,6-dicarboxylic acid (28)—Yield: 29% (23 mg, 0.073 mmol). ¹H NMR (400 MHz, DMSO-*d*₆): δ 8.81 (s, 1H), 7.27 (s, 1H), 7.03 (s, 1H), 6.92-6.81 (m, 3H), 5.99 (s, 2H), 4.45 (d, *J*=5.2 Hz, 2H). ESI-MS(−) calculated for [C₁₅H₁₁N₂O₆][−] *m/z* 315.06, found *m/z* 314.93 [M-H][−].

4-((Thiophen-2-ylmethyl)amino)pyridine-2,6-dicarboxylic acid (29)—Yield: 32% (22 mg, 0.079 mmol). ¹H NMR (400 MHz, DMSO-*d*₆): δ 8.90 (t, *J*=5.6 Hz, 1H), 7.45 (d, *J*=5.2 Hz, 1H), 7.22 (s, 2H), 7.09 (d, *J*=2 Hz, 1H), 7.00 (dd, *J*_F=3.6 Hz, *J*_F=0.8 Hz, 1H), 4.75 (d, *J*=5.6 Hz, 2H). ESI-MS(+) calculated for [C₁₂H₁₁N₂O₄S]⁺ *m/z* 279.04, found *m/z* 279.12 [M+H]⁺, 301.09 [M+Na]⁺, 323.07 [M+H+2Na]⁺.

4-((Furan-2-ylmethyl)amino)pyridine-2,6-dicarboxylic acid (30)—Yield: 52% (34 mg, 0.130 mmol). ¹H NMR (400 MHz, DMSO-*d*₆): δ 7.93 (t, *J*=5.6 Hz, 1H), 7.60 (s, 1H), 7.43 (s, 2H), 6.40 (dd, *J*_F=40 Hz, *J*_F=1.2 Hz, 1H), 6.34 (d, *J*=2.5 Hz, 1H), 4.46 (d, *J*=6 Hz, 2H). ESI-MS(−) calculated for [C₁₂H₉N₂O₅][−] *m/z* 261.05, found *m/z* 261.00 [M-H][−].

Dimethyl 4-hydroxypyridine-2,6-dicarboxylate (31)—4-Hydroxypyridine-2,6-dicarboxylic acid (1 g, 5.46 mmol) was dissolved in MeOH (200 mL) and concentrated H₂SO₄ (0.5 mL) was added to the reaction mixture. The reaction mixture was heated to reflux for 24 h. Once the reaction was completed by TLC, the solvent was removed by evaporation in vacuo to afford **31** as a white powder in 88% yield (1.01 g, 4.78 mmol). No further purification was required. ¹H NMR (400 MHz, MeOD-*d*₄): δ 7.58 (s, 2H), 3.95 (s, 6H). ESI-MS(+) calculated for [C₉H₁₀NO₅]⁺ *m/z* 212.05, found *m/z* 212.07 [M+H]⁺.

Dimethyl 4-bromopyridine-2,6-dicarboxylate (32)—Tetrabutylammonium bromide (6.92 g, 21.45 mmol) and phosphorus pentoxide (3.04 g, 21.45 mmol) were dissolved in dry toluene (20 mL) and the solution was heated to 100°C for 30 min under N₂ atmosphere. Dimethyl 4-hydroxypyridine-2,6-dicarboxylate (1.51 g, 7.15 mmol) was added to the reaction mixture and set to reflux for 3 h. Once the reaction was complete by TLC, the toluene layer was removed. Additional 10 mL of dry toluene was added to the residual brown oil, and heated to reflux for an additional 20 min. The second toluene layer was collected and the combined toluene layers were dried by evaporation in vacuo. The compound was purified by EtOAc and hexane column chromatography, eluting at 45% EtOAc to afford **32** as white crystals in 92% yield (1.8 g, 6.57 mmol). ¹H NMR (400 MHz, DMSO-*d*₆): δ 8.42 (s, 2H), 3.93 (s, 6H). ESI-MS(+) calculated for [C₉H₉BrNO₄]⁺ *m/z* 273.97, found *m/z* 273.98 [M+H]⁺.

General procedure for Para-position Palladium-Catalyzed Cross-Couplings (33–47)

Dimethyl 4-bromopyridine-2,6-dicarboxylate (200 mg, 0.730 mmol, unless otherwise noted), the corresponding boronic acid (1.2 equivalents), and potassium phosphate or potassium acetate (2 equivalents), were dissolved in dry 1,4-dioxane (5 mL). The solution was purged with N₂ gas for 30 min. To this reaction suspension, tetrakis(triphenylphosphine)palladium(0) (0.2 equivalents) was added, and the mixture was heated to reflux at 85°C overnight. The reaction mixture was then filtered through a pad of celite. The organic layer was dried by evaporation in vacuo. The product was purified by

EtOAc and hexane column chromatography. Hydrolysis was performed by dissolving the product in a solution of 1M NaOH (4 mL) and THF (1 mL) at room temperature. Once the reaction was finished by TLC, THF was removed by evaporation in vacuo, and the solution was acidified with 4M HCl to pH 4. The precipitate was collected via vacuum filtration.

4-Phenylpyridine-2,6-dicarboxylic acid (33)—Yield: 68% (120 mg, 0.493 mmol). ¹H NMR (400 MHz, MeOD-*d*₄): δ 8.59 (s, 2H), 7.86-7.84 (m, 2H), 7.60-7.52 (m, 3H). ESI-MS(–) calculated for [C₁₃H₈NO₄][–] *m/z* 242.04, found *m/z* 241.92 [M-H][–].

4-(3-Methoxyphenyl)pyridine-2,6-dicarboxylic acid (34)—Yield: 70% (100 mg, 0.366 mmol). ¹H NMR (400 MHz, MeOD-*d*₄): δ 8.55 (s, 2H), 7.49-7.38 (m, 2H), 7.33 (s, 1H), 7.10 (d, *J*=8 Hz, 1H), 3.90 (s, 3H). ESI-MS(+) calculated for [C₁₄H₁₂NO₅]⁺ *m/z* 274.07, found *m/z* 274.13 [M+H]⁺.

4-(3-Hydroxyphenyl)pyridine-2,6-dicarboxylic acid (35)—Yield: 70% (69 mg, 0.305 mmol). ¹H NMR (400 MHz, DMSO-*d*₆): δ 8.37 (s, 2H), 7.38-7.29 (m, 2H), 7.21 (s, 1H), 6.92 (d, *J*=8 Hz, 1H). ESI-MS(–) calculated for [C₁₃H₈NO₅][–] *m/z* 258.04, found *m/z* 258.36 [M-H][–].

4-(3-Aminophenyl)pyridine-2,6-dicarboxylic acid (36)—Yield: 59% (67 mg, 0.259 mmol). ¹H NMR (400 MHz, MeOD-*d*₄): δ 8.36 (s, 2H), 7.21-7.17 (m, 1H), 7.07 (br s, 1H), 7.00 (d, *J*=8 Hz, 1H), 6.70 (d, *J*=8 Hz, 1H). ESI-MS(–) calculated for [C₁₃H₉N₂O₄][–] *m/z* 257.06, found *m/z* 257.04 [M-H][–].

4-(3-(Dimethylamino)phenyl)pyridine-2,6-dicarboxylic acid (37)—Dimethyl 4-bromopyridine-2,6-dicarboxylate (120 mg, 0.438 mmol). Yield: 70.2% (88 mg, 0.307 mmol). ¹H NMR (400 MHz, DMSO-*d*₆): δ 8.38 (s, 2H), 7.33 (d, *J*=8.7 Hz, 1H), 7.07 (d, *J*=13.2 Hz, 2H), 6.87 (d, *J*=8.3 Hz, 1H), 2.49 (s, 6H). ESI-MS(–) calculated for [C₁₅H₁₃N₂O₄][–] *m/z* 285.09, found *m/z* 285.05 [M-H][–].

4-(2-Methoxyphenyl)pyridine-2,6-dicarboxylic acid (38)—Yield: 84% (100 mg, 0.366 mmol). ¹H NMR (400 MHz, DMSO-*d*₆): δ 8.29 (s, 2H), 7.50-7.46 (m, 2H), 7.20 (d, *J*=8.4 Hz, 1H), 7.12-7.09 (m, 1H), 3.82 (s, 3H). ESI-MS(–) calculated for [C₁₄H₁₀NO₅][–] *m/z* 272.05, found *m/z* 271.91 [M-H][–].

4-(2-Hydroxyphenyl)pyridine-2,6-dicarboxylic acid (39)—Yield: 22% (25 mg, 0.096 mmol). ¹H NMR (400 MHz, DMSO-*d*₆): δ 8.43 (s, 2H), 7.49-7.29 (m, 2H), 7.03-6.94 (m, 2H). ESI-MS(–) calculated for [C₁₃H₈NO₅][–] *m/z* 258.04, found *m/z* 257.97 [M-H][–].

4-(4-Methoxyphenyl)pyridine-2,6-dicarboxylic acid (40)—Yield: 57% (120 mg, 0.418 mmol). ¹H NMR (400 MHz, DMSO-*d*₆): δ 8.37 (s, 2H), 7.89 (d, *J*=8.4 Hz, 2H), 7.10 (d, *J*=8.2 Hz, 2H), 3.83 (s, 3H). ESI-MS(–) calculated for [C₁₄H₁₁NO₅][–] *m/z* 272.06, found *m/z* 271.93 [M-H][–].

4-(4-Hydroxyphenyl)pyridine-2,6-dicarboxylic acid (41)—Yield: 26% (50 mg, 0.192 mmol). ¹H NMR (400 MHz, DMSO-*d*₆): δ 8.35 (s, 2H), 7.77 (s, 2H), 6.92 (d, *J*=8.9 Hz, 2H). ESI-MS(−) calculated for [C₁₃H₈NO₅][−] *m/z* 258.04, found *m/z* 258.04[M-H][−].

4-(4-Aminophenyl)pyridine-2,6-dicarboxylic acid (42)—Yield: 23% (44 mg, 0.170 mmol). ¹H NMR (400 MHz, DMSO-*d*₆): δ 8.42 (s, 2H), 7.91 (d, *J*=8.2 Hz, 2H), 7.22 (d, *J*=8.1 Hz, 2H). ESI-MS(−) calculated for [C₁₃H₉N₂O₄][−] *m/z* 257.06, found *m/z* 256.98[M-H][−].

4-(4-(Dimethylamino)phenyl)pyridine-2,6-dicarboxylic acid (43)—Dimethyl 4-bromopyridine-2,6-dicarboxylate (120 mg, 0.438 mmol). Yield: 40% (50 mg, 0.175 mmol). ¹H NMR (400 MHz, DMSO-*d*₆): δ 8.39 (s, 2H), 8.02 (s, 2H), 6.86 (s, 2H). ESI-MS(−) calculated for [C₁₅H₁₃N₂O₄][−] *m/z* 285.09, found *m/z* 285.04[M-H][−].

4-(3-Carboxyphenyl)pyridine-2,6-dicarboxylic acid (44)—Dimethyl 4-bromopyridine-2,6-dicarboxylate (120 mg, 0.438 mmol). Yield: 45% (57 mg, 0.198 mmol). ¹H NMR (400 MHz, DMSO-*d*₆): δ 8.47 (s, 2H), 8.34 (s, 1H), 8.17 (d, *J*=7.9 Hz, 1H), 8.09 (d, *J*=7.9 Hz, 1H), 7.70 (t, *J*=7.9 Hz, 1H). ESI-MS(−) calculated for [C₁₄H₈NO₆][−] *m/z* 286.04, found *m/z* 285.89 [M-H][−].

4-(3-Acetamidophenyl)pyridine-2,6-dicarboxylic acid (45)—Dimethyl 4-bromopyridine-2,6-dicarboxylate (50 mg, 0.175 mmol). Yield: 57% (30 mg, 0.100 mmol). ¹H NMR (400 MHz, DMSO-*d*₆): δ 8.40 (s, 2H), 8.12 (s, 1H), 7.76 (d, *J*=8.2 Hz, 1H), 8.58 (d, *J*=8.0 Hz, 1H), 7.48 (s, 1H), 2.07 (s, 3H). ESI-MS(−) calculated for [C₁₅H₁₁N₂O₅][−] *m/z* 299.07, found *m/z* 299.00 [M-H][−].

4-(3-Benzamidophenyl)pyridine-2,6-dicarboxylic acid (46)—Dimethyl 4-bromopyridine-2,6-dicarboxylate (50 mg, 0.175 mmol). Yield: 81% (51 mg, 0.141 mmol). ¹H NMR (400 MHz, DMSO-*d*₆): δ 8.43 (s, 2H), 8.31 (s, 1H), 8.05 (d, *J*=8.4 Hz, 1H), 7.99 (d, *J*=7.6 Hz, 2H), 7.66 (d, *J*=7.6 Hz, 1H), 7.61-7.57 (m, 1H), 7.54 (t, *J*=7.4 Hz, 3H). ESI-MS(−) calculated for [C₂₀H₁₃N₂O₅][−] *m/z* 361.08, found *m/z* 361.00 [M-H][−].

4-(3-(2-Phenylacetamido)phenyl)pyridine-2,6-dicarboxylic acid (47)—Dimethyl 4-bromopyridine-2,6-dicarboxylate (50 mg, 0.175 mmol). Yield: 29% (19 mg, 0.050 mmol). ¹H NMR (400 MHz, DMSO-*d*₆): δ 8.37 (d, *J*=0.9 Hz, 2H), 8.12 (d, *J*=2.0 Hz, 1H), 7.77 (ddd, *J*₁=8.0, *J*₂=2.0, *J*₃=1.0 Hz, 1H), 7.59 (dt, *J*₁=7.9, *J*₂=1.3 Hz, 1H), 7.48 (t, *J*=7.9 Hz, 1H), 7.38 – 7.26 (m, 4H), 7.27 – 7.21 (m, 1H), 3.67 (s, 2H). ESI-MS(−) calculated for [C₂₁H₁₅N₂O₅][−] *m/z* 375.10, found *m/z* 374.99 [M-H][−].

Expression and Purification of MBL Metalloforms

NDM-1, IMP-1 and VIM-2 were over-expressed and purified as previously described.^{47,59,60} The Co(II)-substituted metalloform of NDM-1 was generated using the direct addition method, as previously described.⁴⁸

High-Throughput Screening Assay and Z' Factor Determination

Colorimetric, 96-well plate-based assays for the activity of NDM-1, IMP-1 and VIM-2 were established using the substrate chromacef.⁵⁷ Each library compound (50 μM) or a vehicle-only control (DMSO) was incubated for 10 min with each enzyme, NDM-1 (0.2 nM), IMP-1 (0.1 nM) or VIM-2 (1 nM), in 50 mM HEPES, 2 mM CHAPS at pH 7.0 (final assay concentrations). Each reaction was initiated upon addition, with gentle mixing, of the substrate at the following concentrations: 3 μM for NDM-1 (which corresponds to approximately $3 \times K_M$), 7.2 μM for IMP-1 (at K_M), and 16 μM for VIM-2 (at K_M). In the absence of added inhibitors, the increase in absorbance due to formation of the hydrolysis product was followed continuously at 25 °C using a Perkin Elmer Victor 3V 1420 Multilabel Counter plate reader equipped with a 450 nm filter and found to be linear for 20 min. For subsequent screening, a discontinuous assay was used by treating an unmonitored 20 min reaction incubation with addition of EDTA (80 mM), followed by a 3 min incubation, and then reading the final stable absorbance value for each well as described above. The Z' factor determinations³³ were completed using an uninhibited control, and omitting the enzyme as the fully-inhibited control. Low resolution LC-MS was used to analyze the six primary screen hits at the Mass Spectrometry Facility at The University of Texas at Austin.

IC₅₀ Determinations

For initial ranking of the inhibition potency of sublibrary compounds, IC₅₀ values were determined for NDM-1 (and with selected inhibitors for VIM-2 and IMP-1) using the colorimetric substrate chromacef. Stock solutions of each enzyme were diluted using HEPES buffer (50 mM) supplemented with CHAPS (2 mM) at pH 7.0. Steady-state rate parameters were determined for each enzyme in the assay buffer (50 mM HEPES, 1% DMSO at pH 7.0; for IMP-1 only, the assay buffer also contained 2mM CHAPS): NDM-1 ($k_{\text{cat}} = 17 \pm 1 \text{ s}^{-1}$, $K_M = 0.66 \pm 0.07 \mu\text{M}$), VIM-2 ($k_{\text{cat}} = 89 \pm 2 \text{ s}^{-1}$, $K_M = 10.6 \pm 0.6 \mu\text{M}$), IMP-1 ($k_{\text{cat}} = 320 \pm 10 \text{ s}^{-1}$, $K_M = 7 \pm 1 \mu\text{M}$ using $\epsilon_{442\text{nm}} = 14,5000 \text{ M}^{-1}\text{cm}^{-1}$ (Sopharma). IC₅₀ determinations were typically performed in assay buffer using NDM-1 (3 nM), VIM-2 (2 nM), or IMP-1 (0.8 nM), with approximately 20 different inhibitor concentrations. Each reaction contained the following substrate concentrations: 3 μM for NDM-1 (approximately $3 \times K_M$), 14 μM for VIM-2, and 7 μM for IMP-1, (approximately at their respective K_M values). Inhibitor and enzyme are pre-incubated for 20 min (525 μL volume in a 1 mL polystyrene cuvette) and the reaction initiated upon addition of substrate (475 μL volume) and absorbance at 442 nm followed continuously during the linear portion for approximately 0.3 min at 25 °C. Initial velocities are plotted as percent activity with uninhibited enzyme representing 100% and a no-enzyme control as 0 % and fitted to Percent Activity = $100/((1+(\text{IC}_{50}/[\text{I}])^h)$ to obtain IC₅₀ values using KaleidaGraph (Synergy, Reading, PA).

A more sensitive, continuous, fluorescent, 96-well plate-based assay with a larger signal and longer linear assay window was used to rank the potency of the more potent compounds found in sublibrary 3. Typically, inhibitor stock solutions (50 mM in DMSO) were diluted in DMSO to 5 mM and used to prepare five sub-stock solutions of each inhibitor spanning between 500 μM and 50 nM in assay buffer (50 mM HEPES, 2 mM CHAPS at pH 7.0), and then arrayed as 20 μL aliquots, with addition of assay buffer to reach a final inhibitor assay

concentration between 100 μM and 1 nM, into a round-bottomed, untreated black polypropylene 96-well plate (Corning). Enzyme (NDM-1 at 41.7 pM) was added in a volume of 60 μL and incubated for 20 min after briefly shaking. Full activity (no added inhibitor) controls were performed by substituting 20 μL of assay buffer for the inhibitor solution, and no-enzyme controls (to monitor background hydrolysis rates of substrate) were performed in a total of 80 μL assay buffer. Next, the fluorocillin substrate was added in a 20 μL aliquot (from a 433 nM stock solution prepared immediately in assay buffer prior to use) to initiate the reaction. Fluorocillin green has a difluorofluorescein core coupled to two cefalotin groups that serve as a substrate for β -lactamases and hydrolysis can be followed by monitoring changes in fluorescence at $\lambda_{\text{ex/em}}$ 495/525 nm.^{16,39} The automatic shaking feature of the PerkinElmer Victor ³V fluorescent plate reader was used to mix the samples for 5 s and fluorescence is determined during a 1 s interval for each well and then repeated 10 times over the duration of the assay, typically 25 min, during which linear rates are observed. The rates of fluorescence increase are determined and IC_{50} values determined as described above for the chromogenic assay. Final assay concentrations were NDM-1 (25 pM), or VIM-2 (250 pM) and IMP-1 (5 pM), and fluorocillin (87 nM) in HEPES buffer (50 mM), CHAPS (2 mM in IMP-1 assays only), at pH 7.0. Periodically, selected sublibrary compounds were assayed independently in two separate laboratories (SMC, WF) to validate the rank order of compound potency.

Inhibitor Selectivity Studies

MMP-2/MMP-12 Assays^{45,46}—MMP-2 and -12, and OmniMMP fluorogenic substrate were purchased from Enzo Life Sciences (Farmingdale, NY, USA). The assays were carried out in black 96-well plates (Corning). Each well contained a volume of 100 μL including buffer (50 mM HEPES, 10 mM CaCl_2 , 0.05% Brij-35, pH 7.5), human recombinant MMP (1.16 U/well of MMP-2, 0.007 U/well of MMP-12, Enzo Life Sciences), inhibitor (various concentrations, 1 mM – 5 μM), and fluorogenic OmniMMP substrate (4 μM Mca-Pro-LeuGly-Leu-Dpa-Ala-Arg- NH_2 •AcOH, Enzo Life Sciences). The enzyme and inhibitor were incubated in solution at 37 $^\circ\text{C}$ for 30 min, followed by the addition of the substrate to initiate the reaction. The change in fluorescence was monitored over 20 min with excitation and emission wavelengths at 320 and 400 nm, respectively. The negative control wells, containing no inhibitor, were arbitrarily set as 100% activity. The positive control wells, containing 200 μM NSA, were arbitrarily set as 0% activity. MMP activity was defined as the ratio of fluorescence increase in the inhibitor wells relative to the negative control wells, expressed as a percentage. The assays were performed in triplicate.

HDAC-1/HDAC-6 Assays—HDAC-1 and -6 were purchased from BPS Bioscience (BPS Bioscience catalog #50051 and 50006, San Diego, CA, USA) and the assay was carried out as instructed by manufacturer. The assays were carried out in black 96-well plates (Costar). Each well contained a volume of 50 μL including buffer (25 mM Tris/HCl, 137 mM NaCl, 2.7 mM KCl, 1 mM MgCl_2 , 0.1 mg/mL BSA, pH 8.0), HDAC (3.8 ng/well of HDAC-1, 50 ng/well of HDAC-6, BPS Bioscience, catalogue no. 50051 and no. 50006, respectively), inhibitor (various concentrations, 1 mM – 5 μM), and HDAC substrate 3 (20 μM , BPS Bioscience, catalogue no. 50037). Prior to adding substrate, the plate was preincubated for 5 min. Upon addition of substrate, the plate was incubated at 37 $^\circ\text{C}$ for 30 min. HDAC assay

developer (50 μ L, BPS Bioscience, catalogue no. 50030) was added to each well and the plate incubated for 15 min at room temperature. The fluorescence was recorded at excitation and emission wavelengths of 360 and 460 nm, respectively. The negative control wells, containing no inhibitor, were arbitrarily set as 100% activity. The positive control wells, containing 200 μ M SAHA, were arbitrarily set as 0% activity. HDAC activity was defined as the ratio of fluorescence in the inhibitor wells relative to the negative control wells, expressed as a percentage. The assays were performed in triplicate.

hCAII Assays⁶¹—Human carbonic anhydrase II was expressed and purified as previously described.⁶² Assays were carried out in clear 96-well plates (Costar). Each well contained a volume of 100 μ L including buffer (50 mM HEPES, pH = 8.0), hCAII (100 nM), inhibitor (various concentrations, 1 mM – 5 μ M), and *p*-nitrophenyl acetate (500 μ M). The enzyme and inhibitor were incubated in solution at 30 °C for 10 min prior to the addition of the *p*-nitrophenyl acetate to initiate the reaction. The change in absorbance was monitored for 15 min at 405 nm. The negative control wells, containing no inhibitor, were arbitrarily set as 100% activity. The positive control wells, containing 50 μ M benzene sulfonamide, were arbitrarily set as 0% activity. Activity was defined as the ratio of color shift in the inhibitor wells relative to the negative control wells, expressed as a percentage. The assays were performed in triplicate.

¹H NMR Spectroscopy

Metal-free, apo-NDM-1 was concentrated to ~1 mM with an Amicon Ultra-4 Centrifugal Unit with an Ultracel-10 membrane. To the concentrated protein, 2 equivalents of CoCl₂ were added. Each NMR sample was buffered with 50 mM HEPES, 150 mM NaCl, 10% D₂O at pH 6.8. Tested compounds were dissolved in DMSO at high concentration (50 – 100 mM) so they could be titrated in ~5 μ L aliquots. Spectra were collected at 292 K on a Bruker ASX300 (BBI probe) ¹H NMR operating at a frequency of 300.16 MHz. Spectra were collected using a frequency-switching method, applying a long, low power (270 ms) pulse centered at the water frequency, followed by a high power 3 μ s pulse centered at 90 ppm.⁶³ This method allows for suppression of the water signal with enhancement of severely hyperfine shifted resonances. Spectra consisted of 30,000 transients of 16k data points over a 333 ppm spectral window (t_{aq} ~51 ms); signal averaging took ~3 h per spectrum.

EPR Spectroscopy

Samples containing 1 molar equivalent of compound of interest added to CoCo-NDM-1, and CoCo-NDM-1 in the absence of compound, included ~10 % (v/v) glycerol as glassing agent. Samples were loaded into EPR tubes, degassed by repeated evacuation/purgation with N₂, prior to data collection. Spectra were collected on a Bruker EMX EPR spectrometer, equipped with an ER4116-DM dual mode resonator (9.37 GHz, parallel; 9.62 GHz perpendicular). The data in Figure 4 were scaled so that the x-axes matched (perpendicular mode field values were scaled by 9.37/9.62). Temperature control was accomplished using an Oxford ESR900 cryostat and temperature controller. Other spectral conditions included: microwave power = 0.2 mW; field modulation = 10 G (100 kHz); receiver gain = 10⁴; time constant/conversion time = 41 ms.

UV-Vis Spectroscopy

Apo-NDM-1 was diluted to 300 μM in 50 mM HEPES, pH 6.8 containing 150 mM NaCl. Two molar equivalents of CoCl_2 were added to the protein from a 50 mM stock solution. The resulting diCo(II)-substituted NDM-1 enzyme was separated into 500 μL aliquots. To each aliquot, between 0 – 600 μM of the compound of interest was added. The compound stock concentrations were 20 mM. L-captopril, DPA, and **36** stocks were dissolved in DMSO, and the EDTA stock was dissolved in water. The samples were then incubated on ice for 30 min. The samples were added to a 500 μL quartz cuvette and UV-Vis spectra were collected on a PerkinElmer Lambda 750 UV/VIS/NIR Spectrometer measuring absorbance between 300 to 700 nm at 25 $^\circ\text{C}$. A blank spectrum of 50 mM HEPES, pH 6.8 containing 150 mM NaCl was used to generate difference spectra. All data was normalized at 700 nm.

Equilibrium Dialysis

NDM-1 (final concentration 8 μM) in 5 mL of 50 mM HEPES at pH 7.5, was mixed with the compound of interest at concentrations from 0 – 128 μM . After incubation for 30 min, the solutions were dialyzed versus 500 mL of metal-free, 50 mM HEPES at pH 7.5, for 4 hours (dialysis tubing MWCO 6000–8000, Fisherbrand). The Zn(II) content in the resulting NDM-1 samples was determined using Inductively Coupled Plasma with Atomic Emission Spectroscopy (ICP-AES, Perkin Elmer Optima 7300DV). The emission wavelength was set to 213.856 nm, as previously described.^{47,48}

Fluorescence Emission Studies

NDM-1 (final concentration 2 μM) in 2 mL of 50 mM HEPES at pH 7.5, was mixed with the compound of interest at concentrations from 4 – 32 μM . After incubation for 30 min, fluorescence emission spectra of NDM-1 samples were obtained on a Perkin Elmer Luminescence spectrometer (Model LS-55), with an excitation wavelength of 280 nm and an emission spectrum from 300 to 400 nm. The relative tryptophan fluorescence intensity (at 348 nm) was calculated setting the intensity of HEPES buffer 0% and NDM-1 containing no inhibitors at 100%. L-Tryptophan (2 μM) was used in place of NDM-1 as a control.

Microdilution Broth Minimum Inhibitory Concentrations (MICs)

MICs were performed in triplicate in Mueller-Hinton (MH) broth according to CLSI guidelines.⁶⁴ Overnight cultures of *E. coli* and *K. pneumoniae* clinical isolates expressing *bla*_{NDM-1}⁵³ were inoculated into 5 mL MH broth to $\text{OD}_{600} = 0.1$ and grown to $\text{OD}_{600} = 0.224$ (approximately $1\text{--}2 \times 10^8$ CFU/mL). These cultures were diluted (3 μL + 4997 μL MH) and 100 μL inoculated into each well of a 96-well plate containing 100 μL of serial dilutions of imipenem (Fresenius Kabi, Lake Zurich, IL) with or without added compound **36** (100 mg/L). Compound **36** alone was included as a control. The plates were placed in a 37 $^\circ\text{C}$ incubator for 18–20 hours and wells checked for growth.

Cytotoxicity Assay

HEK293 cells were plated at 10,000 cells/well in a clear bottom black walled 96-well plate 12 h prior to treatment with either vehicle (DMSO) or compound **36** (n=6 per treatment per time point). Cells were incubated with DMSO or **36** for 4 and 24 h in 100 μL of Dulbecco's

Modified Eagle Medium supplemented with 10% EquafETAL (Atlas Biologicals) and Penicillin-Streptomycin (Sigma-Aldrich). Cell-titer blue reagent (Promega) was added after either 4 or 24 h incubation with DMOS or **36** and incubated for and addition 1 hour prior to being read on a Victor3V spectrophotometer (536ex/595em). Graphs were created using GraphPad Prism and significance was calculated using an ANOVA followed by a Tukey's post-hoc analysis (Figure S8). A cell viability of 1.0 (100%) was defined by the vehicle only (DMSO) control.

Cell Imaging

HEK293 cells were treated as described in the cytotoxicity assay and imaged with using a NIKON EclipseTi epifluorescent microscope using 20X magnification (Figure S9).

Supplementary Material

Refer to Web version on PubMed Central for supplementary material.

Acknowledgments

We thank Prof. Edward M. Mills for assistance with the mammalian cell studies. We also thank Dr. Yongxuan Su for mass spectrometry sample analysis at The Molecular Mass Spectrometry Facility at UC San Diego and Dr. Le Wang for assistance with SXR structure determination. This work was supported in part by the National Institutes of Health (GM111926), the National Science Foundation (CHE-1509285 to M.W.C. and D.L.T.), and by the Robert A. Welch Foundation (F-1572 to W.F.). S.M.C. is a co-founder of and has an equity interest in Cleave Biosciences and Forge Therapeutics, companies that may potentially benefit from the research results. S.M.C. also serves on the Scientific Advisory Board for these companies. The terms of this arrangement have been reviewed and approved by the University of California, San Diego in accordance with its conflict of interest policies. Research reported in this publication was supported in part by the National Institute of Allergy and Infectious Diseases of the National Institutes of Health under Award Numbers R01AI100560, R01AI063517, and R01AI072219 to RAB, T32-GM-7250 to Case Western Reserve University, MLW. This study was supported in part by funds and/or facilities provided by the Cleveland Department of Veterans Affairs, Award Number 1101BX001974 to RAB from the Biomedical Laboratory Research & Development Service of the VA Office of Research and Development and the Geriatric Research Education and Clinical Center VISN 10 to RAB. The content is solely the responsibility of the authors and does not necessarily represent the official views of the National Institutes of Health or the Department of Veterans Affairs.

ABBREVIATIONS

MBP	Metal Binding Pharmacophores
MBL	Metallo- β -lactamase
NDM-1	New Delhi Metallo- β -lactamase
VIM-2	Verona Integrin-encoded Metallo- β -lactamase-2
IMP-1	imipenemase-1
DPA	Dipicolinic acid
EDTA	Ethylenediaminetetraacetic acid
EPR	Electron Paramagnetic Resonance
MIC	Minimum Inhibitory Concentration

References

1. Brown DG, Wright GD. Antibacterial drug discovery in the resistance era. *Nature*. 2016; 529:336–343. [PubMed: 26791724]
2. Bush K, Jacoby GA. Updated functional classification of beta-lactamases. *Antimicrob Agents Chemother*. 2010; 54:969–976. [PubMed: 19995920]
3. Drawz SM, Bonomo RA. Three decades of beta-lactamase inhibitors. *Clin Microbiol Rev*. 2010; 23:160–201. [PubMed: 20065329]
4. Crowder MW, Spencer J, Vila AJ. Metallo-beta-lactamases: novel weaponry for antibiotic resistance in bacteria. *Acc Chem Res*. 2006; 39:721–728. [PubMed: 17042472]
5. Walsh TR. Emerging carbapenemases: a global perspective. *Int J Antimicrob Agents*. 2010; 36:8–14.
6. Yong D, Toleman MA, Giske CG, Cho HS, Sundman K, Lee K, Walsh TR. Characterization of a new metallo-beta-lactamase gene, bla(NDM-1), and a novel erythromycin esterase gene carried on a unique genetic structure in *Klebsiella pneumoniae* sequence type 14 from India. *Antimicrob Agents Chemother*. 2009; 53:5046–5054. [PubMed: 19770275]
7. Nordmann P, Poirel L, Toleman MA, Walsh TR. Does broad-spectrum beta-lactam resistance due to NDM-1 herald the end of the antibiotic era for treatment of infections caused by Gram-negative bacteria? *J Antimicrob Chemother*. 2011; 66:689–692. [PubMed: 21393184]
8. Kumarasamy KK, Toleman MA, Walsh TR, Bagaria J, Butt F, Balakrishnan R, Chaudhary U, Doumith M, Giske CG, Irfan S, Krishnan P, Kumar AV, Maharjan S, Mushtaq S, Noorie T, Paterson DL, Pearson A, Perry C, Pike R, Rao B, Ray U, Sarma JB, Sharma M, Sheridan E, Thirunarayan MA, Turton J, Upadhyay S, Warner M, Welfare W, Livermore DM, Woodford N. Emergence of a new antibiotic resistance mechanism in India, Pakistan, and the UK: a molecular, biological, and epidemiological study. *Lancet Infect Dis*. 2010; 10:597–602. [PubMed: 20705517]
9. Mojica MF, Bonomo RA, Fast W. B1-metallo-beta-lactamases: where do we stand? *Curr Drug Targets*. 2016; 17:1029–1050. [PubMed: 26424398]
10. Aoki N, Ishii Y, Tateda K, Saga T, Kimura S, Kikuchi Y, Kobayashi T, Tanabe Y, Tsukada H, Gejyo F, Yamaguchi K. Efficacy of calcium-EDTA as an inhibitor for metallo-beta-lactamase in a mouse model of *Pseudomonas aeruginosa* pneumonia. *Antimicrob Agents Chemother*. 2010; 54:4582–4588. [PubMed: 20713659]
11. Yoshizumi A, Ishii Y, Livermore DM, Woodford N, Kimura S, Saga T, Harada S, Yamaguchi K, Tateda K. Efficacies of calcium-EDTA in combination with imipenem in a murine model of sepsis caused by *Escherichia coli* with NDM-1 beta-lactamase. *J Infect Chemother*. 2013; 19:992–995. [PubMed: 23233082]
12. King AM, Reid-Yu SA, Wang W, King DT, De Pascale G, Strynadka NC, Walsh TR, Coombes BK, Wright GD. Aspergillomarasmine A overcomes metallo-beta-lactamase antibiotic resistance. *Nature*. 2014; 510:503–506. [PubMed: 24965651]
13. King DT, Worrall LJ, Gruninger R, Strynadka NC. New Delhi metallo-beta-lactamase: structural insights into beta-lactam recognition and inhibition. *J Am Chem Soc*. 2012; 134:11362–11365. [PubMed: 22713171]
14. Guo Y, Wang J, Niu G, Shui W, Sun Y, Zhou H, Zhang Y, Yang C, Lou Z, Rao Z. A structural view of the antibiotic degradation enzyme NDM-1 from a superbug. *Protein Cell*. 2011; 2:384–394. [PubMed: 21637961]
15. Li N, Xu Y, Xia Q, Bai C, Wang T, Wang L, He D, Xie N, Li L, Wang J, Zhou HG, Xu F, Yang C, Zhang Q, Yin Z, Guo Y, Chen Y. Simplified captopril analogues as NDM-1 inhibitors. *Bioorg Med Chem Lett*. 2014; 24:386–389. [PubMed: 24269122]
16. Klingler FM, Wichelhaus TA, Frank D, Cuesta-Bernal J, El-Delik J, Muller HF, Sjuts H, Gottig S, Koenigs A, Pos KM, Pogoryelov D, Proschak E. Approved drugs containing thiols as inhibitors of metallo-beta-lactamases: strategy to combat multidrug-resistant bacteria. *J Med Chem*. 2015; 58:3626–3630. [PubMed: 25815530]
17. Garcia-Saez I, Hopkins J, Papamicael C, Franceschini N, Amicosante G, Rossolini GM, Galleni M, Frere JM, Dideberg O. The 1.5-Å structure of *Chryseobacterium meningosepticum* zinc beta-

- lactamase in complex with the inhibitor, D-captopril. *J Biol Chem.* 2003; 278:23868–23873. [PubMed: 12684522]
18. Jaffe IA. Adverse effects profile of sulfhydryl compounds in man. *Am J Med.* 1986; 80:471–476. [PubMed: 2937293]
 19. Kitamura K, Aihara M, Osawa J, Naito S, Ikezawa Z. Sulfhydryl drug-induced eruption: a clinical and histological study. *J Dermatol.* 1990; 17:44–51. [PubMed: 2139441]
 20. Brem J, Cain R, Cahill S, McDonough MA, Clifton II, Jimenez-Castellanos JC, Avison MB, Spencer J, Fishwick CW, Schofield CJ. Structural basis of metallo-beta-lactamase, serine-beta-lactamase and penicillin-binding protein inhibition by cyclic boronates. *Nat Commun.* 2016; 7:12406. [PubMed: 27499424]
 21. Fast W, Sutton LD. Metallo-beta-lactamase: inhibitors and reporter substrates. *Biochim Biophys Acta.* 2013; 1834:1648–1659. [PubMed: 23632317]
 22. Gonzalez MM, Kosmopoulou M, Mojica MF, Castillo V, Hinchliffe P, Pettinati I, Brem J, Schofield CJ, Mahler G, Bonomo RA, Llarrull LI, Spencer J, Vila AJ. Bisthiazolidines: a substrate-mimicking scaffold as an inhibitor of the NDM-1 carbapenemase. *ACS Infect Dis.* 2015; 1:544–554. [PubMed: 27623409]
 23. Hinchliffe P, Gonzalez MM, Mojica MF, Gonzalez JM, Castillo V, Saiz C, Kosmopoulou M, Tooke CL, Llarrull LI, Mahler G, Bonomo RA, Vila AJ, Spencer J. Cross-class metallo-beta-lactamase inhibition by bisthiazolidines reveals multiple binding modes. *Proc Natl Acad Sci U S A.* 2016; 113:3745–3754.
 24. Zartler, E., Shapiro, M. *Designing a Fragment Process to Fit Your Needs In Fragment-based Drug Discovery: A Practical Approach.* John Wiley & Sons; Chichester, UK: 2008.
 25. Garau G, Garcia-Saez I, Bebrone C, Anne C, Mercuri P, Galleni M, Frere JM, Dideberg O. Update of the standard numbering scheme for class B beta-lactamases. *Antimicrob Agents Chemother.* 2004; 48:2347–2349. [PubMed: 15215079]
 26. Agrawal A, de Oliveira CA, Cheng Y, Jacobsen JA, McCammon JA, Cohen SM. Thioamide hydroxypyrothiones supersede amide hydroxypyrothiones in potency against anthrax lethal factor. *J Med Chem.* 2009; 52:1063–1074. [PubMed: 19170530]
 27. Agrawal A, Johnson SL, Jacobsen JA, Miller MT, Chen LH, Pellicchia M, Cohen SM. Chelator fragment libraries for targeting metalloproteinases. *ChemMedChem.* 2010; 5:195–199. [PubMed: 20058293]
 28. Lewis JA, Mongan J, McCammon JA, Cohen SM. Evaluation and binding-mode prediction of thiopyrone-based inhibitors of anthrax lethal factor. *ChemMedChem.* 2006; 1:694–697. [PubMed: 16902919]
 29. Puerta DT, Schames JR, Henchman RH, McCammon JA, Cohen SM. From model complexes to metalloprotein inhibition: a synergistic approach to structure-based drug discovery. *Angew Chem Int Ed Engl.* 2003; 42:3772–3774. [PubMed: 12923840]
 30. Puerta DT, Mongan J, Tran BL, McCammon JA, Cohen SM. Potent, selective pyrone-based inhibitors of stromelysin-1. *J Am Chem Soc.* 2005; 127:14148–14149. [PubMed: 16218585]
 31. Rouffet M, de Oliveira CA, Udi Y, Agrawal A, Sagi I, McCammon JA, Cohen SM. From sensors to silencers: quinoline- and benzimidazole-sulfonamides as inhibitors for zinc proteases. *J Am Chem Soc.* 2010; 132:8232–8233. [PubMed: 20507095]
 32. Copeland RA. Evaluation of enzyme inhibitors in drug discovery. A guide for medicinal chemists and pharmacologists. *Methods Biochem Anal.* 2005; 46:1–265. [PubMed: 16350889]
 33. Zhang JH, Chung TD, Oldenburg KR. A simple statistical parameter for use in evaluation and validation of high throughput screening assays. *J Biomol Screen.* 1999; 4:67–73. [PubMed: 10838414]
 34. Schlesinger SR, Bruner B, Farmer PJ, Kim SK. Kinetic characterization of a slow-binding inhibitor of Bla2: thiomaltol. *J Enzyme Inhib Med Chem.* 2013; 28:137–142. [PubMed: 22233540]
 35. Hanaya K, Suetsugu M, Saijo S, Yamato I, Aoki S. Potent inhibition of dinuclear zinc(II) peptidase, an aminopeptidase from *Aeromonas proteolytica*, by 8-quinolinol derivatives: inhibitor design based on Zn²⁺ fluorophores, kinetic, and X-ray crystallographic study. *J Biol Inorg Chem.* 2012; 17:517–529. [PubMed: 22311113]

36. Horsfall LE, Garau G, Lienard BM, Dideberg O, Schofield CJ, Frere JM, Galleni M. Competitive inhibitors of the CphA metallo-beta-lactamase from *Aeromonas hydrophila*. *Antimicrob Agents Chemother*. 2007; 51:2136–2142. [PubMed: 17307979]
37. Aitha M, Moller AJ, Sahu ID, Horitani M, Tierney DL, Crowder MW. Investigating the position of the hairpin loop in New Delhi metallo-beta-lactamase, NDM-1, during catalysis and inhibitor binding. *J Inorg Biochem*. 2016; 156:35–39. [PubMed: 26717260]
38. Okabe N, Oya N. Copper(II) and zinc(II) complexes of pyridine-2,6-dicarboxylic acid. *Acta Crystallogr, Sect C: Struct Chem*. 2000; 56(Pt 3):305–307.
39. Rukavishnikov A, Gee KR, Johnson I, Corry S. Fluorogenic cephalosporin substrates for beta-lactamase TEM-1. *Anal Biochem*. 2011; 419:9–16. [PubMed: 21867672]
40. Hopkins AL, Groom CR, Alex A. Ligand efficiency: a useful metric for lead selection. *Drug Discovery Today*. 2004; 9:430–431. [PubMed: 15109945]
41. Brown DG, May-Dracka TL, Gagnon MM, Tommasi R. Trends and exceptions of physical properties on antibacterial activity for Gram-positive and Gram-negative pathogens. *J Med Chem*. 2014; 57:10144–10161. [PubMed: 25402200]
42. Gregoretti IV, Lee YM, Goodson HV. Molecular evolution of the histone deacetylase family: functional implications of phylogenetic analysis. *J Mol Biol*. 2004; 338:17–31. [PubMed: 15050820]
43. Devel L, Rogakos V, David A, Makaritis A, Beau F, Cuniasse P, Yiotakis A, Dive V. Development of selective inhibitors and substrate of matrix metalloproteinase-12. *J Biol Chem*. 2006; 281:11152–11160. [PubMed: 16481329]
44. Sly WS, Hu PY. Human carbonic anhydrases and carbonic anhydrase deficiencies. *Annu Rev Biochem*. 1995; 64:375–401. [PubMed: 7574487]
45. Day JA, Cohen SM. Investigating the selectivity of metalloenzyme inhibitors. *J Med Chem*. 2013; 56:7997–8007. [PubMed: 24074025]
46. Chen Y, Cohen SM. Investigating the selectivity of metalloenzyme inhibitors in the presence of competing metalloproteins. *ChemMedChem*. 2015; 10:1733–1738. [PubMed: 26412596]
47. Yang H, Aitha M, Hetrick AM, Richmond TK, Tierney DL, Crowder MW. Mechanistic and spectroscopic studies of metallo-beta-lactamase NDM-1. *Biochemistry*. 2012; 51:3839–3847. [PubMed: 22482529]
48. Yang H, Aitha M, Marts AR, Hetrick A, Bennett B, Crowder MW, Tierney DL. Spectroscopic and mechanistic studies of heterodimetallic forms of metallo-beta-lactamase NDM-1. *J Am Chem Soc*. 2014; 136:7273–7285. [PubMed: 24754678]
49. Selleck C, Larrabee JA, Harmer J, Guddat LW, Miti N, Helweh W, Ollis DL, Craig WR, Tierney DL, Monteiro Pedroso M, Schenk G. AIM-1: an antibiotic-degrading metallohydrolase that displays mechanistic flexibility. *Chem Eur J*. 2016; 22:17704–17714. [PubMed: 27778387]
50. Bennett, B. *Metals in Biology: Applications of High-resolution EPR to Metalloenzymes*. Hanson, G., Berliner, L., editors. Springer New York; New York, NY: 2010. p. 345-370.
51. Crowder MW, Yang KW, Carenbauer AL, Periyannan G, Seifert ME, Rude NE, Walsh TR. The problem of a solvent exposable disulfide when preparing Co(II)-substituted metallo-beta-lactamase L1 from *Stenotrophomonas maltophilia*. *J Biol Inorg Chem*. 2001; 6:91–99. [PubMed: 11191226]
52. Krezel A, Maret W. The biological inorganic chemistry of zinc ions. *Arch Biochem Biophys*. 2016; 611:3–19. [PubMed: 27117234]
53. Lascols C, Hackel M, Marshall SH, Hujer AM, Bouchillon S, Badal R, Hoban D, Bonomo RA. Increasing prevalence and dissemination of NDM-1 metallo-β-lactamase in India: data from the SMART study (2009). *J Antimicrob Chemother*. 2011; 66:1992–1997. [PubMed: 21676902]
54. Christopheit T, Carlsen TJ, Helland R, Leiros HK. Discovery of novel inhibitor scaffolds against the metallo-β-lactamase VIM-2 by surface plasmon resonance (SPR) based fragment screening. *J Med Chem*. 2015; 58:8671–8682. [PubMed: 26477515]
55. Christopheit T, Leiros HK. Fragment-based discovery of inhibitor scaffolds targeting the metallo-β-lactamases NDM-1 and VIM-2. *Bioorg Med Chem Lett*. 2016; 26:1973–1977. [PubMed: 26976213]

56. Klingler FM, Moser D, Buttner D, Wichelhaus TA, Lohr F, Dotsch V, Proschak E. Probing metallo-beta-lactamases with molecular fragments identified by consensus docking. *Bioorg Med Chem Lett.* 2015; 25:5243–5246. [PubMed: 26463134]
57. Yu S, Vosbeek A, Corbella K, Severson J, Schesser J, Sutton LD. A chromogenic cephalosporin for beta-lactamase inhibitor screening assays. *Anal Biochem.* 2012; 428:96–98. [PubMed: 22709853]
58. Perez C, Monserrat JP, Chen Y, Cohen SM. Exploring hydrogen peroxide responsive thiazolidinone-based prodrugs. *Chem Commun.* 2015; 51:7116–7119.
59. Griffin DH, Richmond TK, Sanchez C, Moller AJ, Breece RM, Tierney DL, Bennett B, Crowder MW. Structural and kinetic studies on metallo-beta-lactamase IMP-1. *Biochemistry.* 2011; 50:9125–9134. [PubMed: 21928807]
60. Aitha M, Marts AR, Bergstrom A, Moller AJ, Moritz L, Turner L, Nix JC, Bonomo RA, Page RC, Tierney DL, Crowder MW. Biochemical, mechanistic, and spectroscopic characterization of metallo-beta-lactamase VIM-2. *Biochemistry.* 2014; 53:7321–7331. [PubMed: 25356958]
61. Martin DP, Cohen SM. Nucleophile recognition as an alternative inhibition mode for benzoic acid based carbonic anhydrase inhibitors. *Chem Commun.* 2012; 48:5259–5261.
62. Monnard FW, Heinisch T, Nogueira ES, Schirmer T, Ward TR. Human carbonic anhydrase II as a host for piano-stool complexes bearing a sulfonamide anchor. *Chem Commun.* 2011; 47:8238–8240.
63. Riley EA, Petros AK, Smith KA, Gibney BR, Tierney DL. Frequency-switching inversion-recovery for severely hyperfine-shifted NMR: evidence of asymmetric electron relaxation in high-spin Co(II). *Inorg Chem.* 2006; 45:10016–10018. [PubMed: 17140197]
64. CLSI M07-A10. 2. Vol. 35. Clinical and Laboratory Standards Institute; Wayne, PA, United States: 2015.

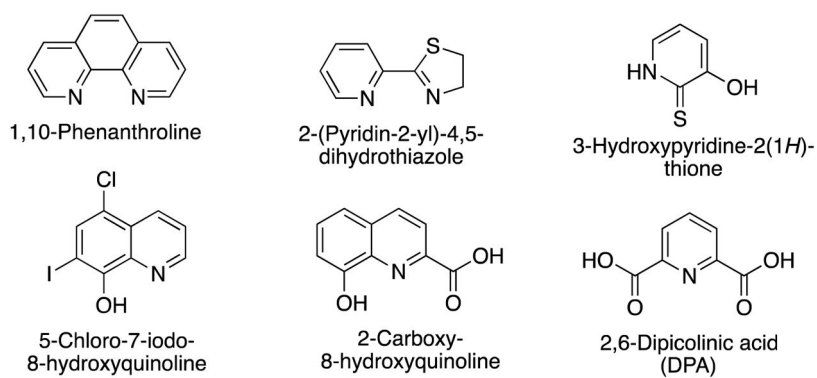


Figure 1. Primary screening hits observed to inhibit all three B1 MBLs tested: NDM-1, IMP-1, and VIM-2. See Table S1 for detailed percent inhibition values.

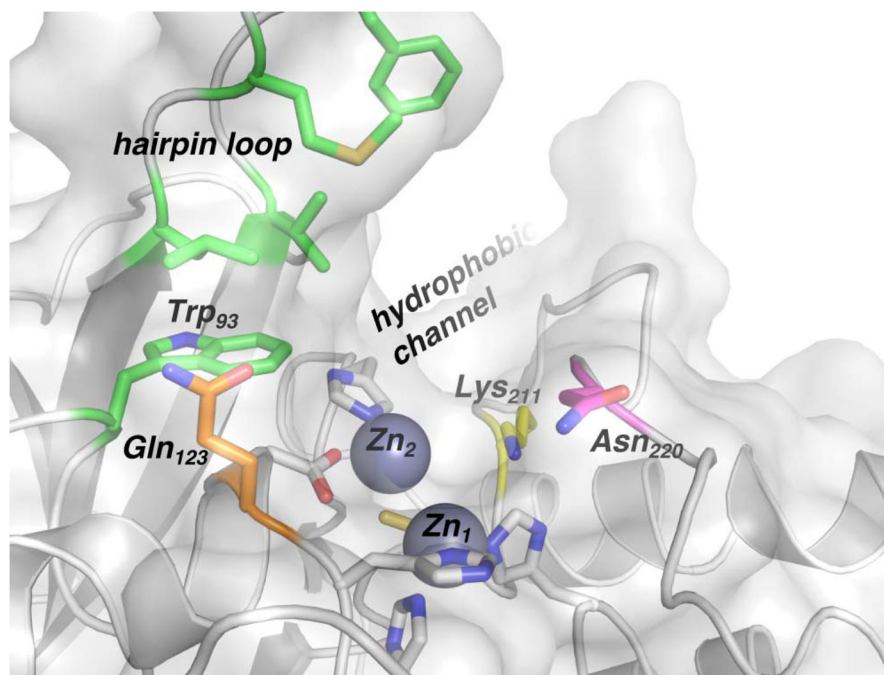


Figure 2. Active-site pocket of NDM-1. A ribbon diagram of NDM-1 covered by a transparent surface depicts a shallow hydrophobic channel flanking the di-Zn(II) site (gray spheres). Selected residues are shown in stick form, including the residues ligating the Zn(II) ions (gray), hydrophobic residues in the neighboring β -hairpin loop (green), residues with the potential to interact with an inhibitor via hydrogen-bonding (purple and orange), and a conserved Lys211 (yellow). All heteroatoms are colored by type (blue for nitrogen, red for oxygen, gold for sulfur). The figure was prepared with coordinates from Protein Data Bank accession code 3Q6X, chain A, omitting the hydrolyzed ampicillin product.

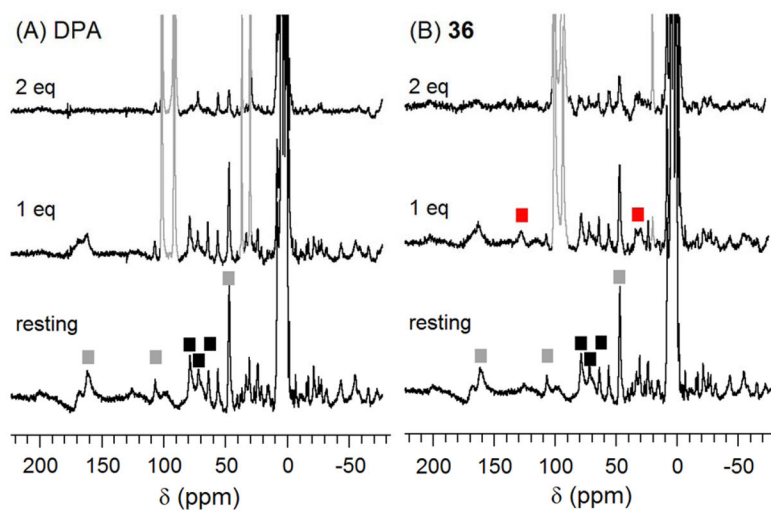


Figure 3. 300 MHz ^1H NMR titrations of CoCo-NDM-1 with (A) DPA and (B) **36**. Resonances assigned to Zn_1 site ligands are marked with black squares, while those assigned to Zn_2 ligands are marked with gray squares. Resonances indicative of a ternary complex are marked with red squares.

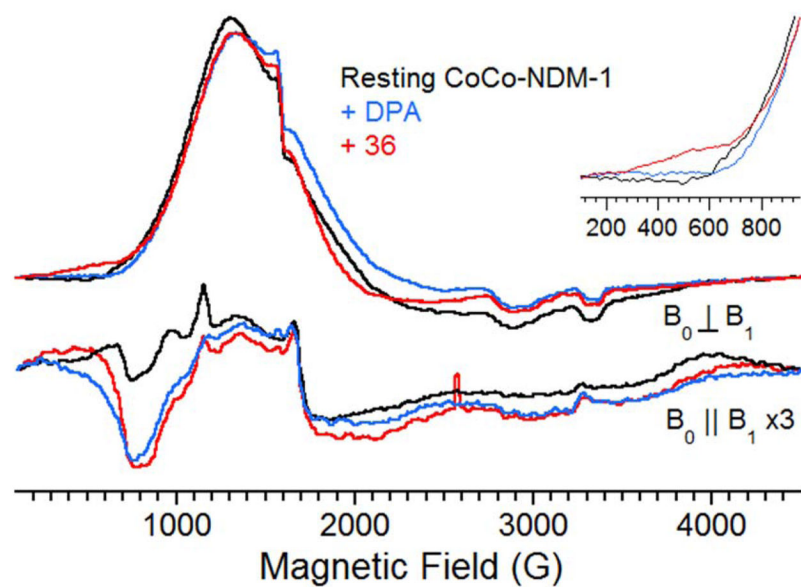


Figure 4. X-band EPR spectroscopy of CoCo-NDM-1 (black) and CoCo-NDM-1 with 1 equivalent of added DPA (blue) and **36** (red). Standard perpendicular mode spectra are on top, parallel mode spectra (scaled 3-fold) are shown below. Inset: Expansion of the low-field region of the perpendicular mode spectra.

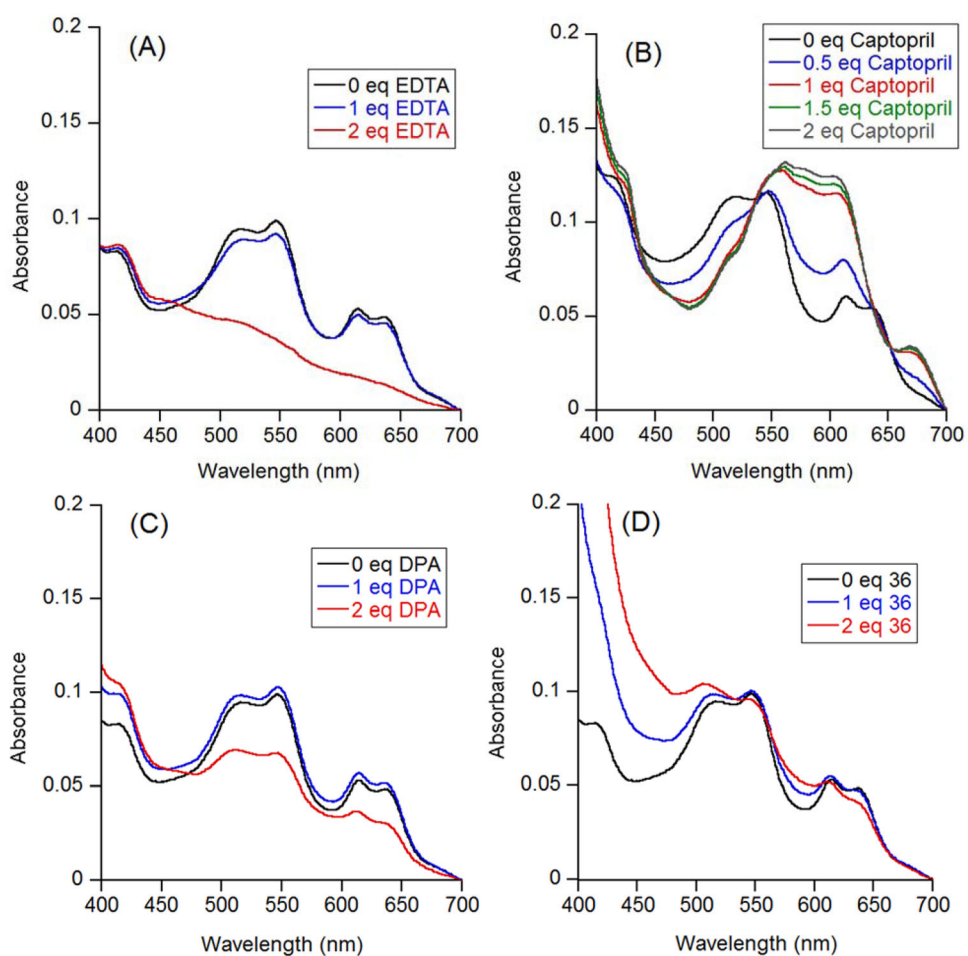


Figure 5. UV-Vis spectroscopy of CoCo-NDM-1 (black lines) and CoCo-NDM-1 (300 μ M) with EDTA (A) and L-captopril (B) as control, and 1–2 equivalents of added DPA (C), and **36** (D).

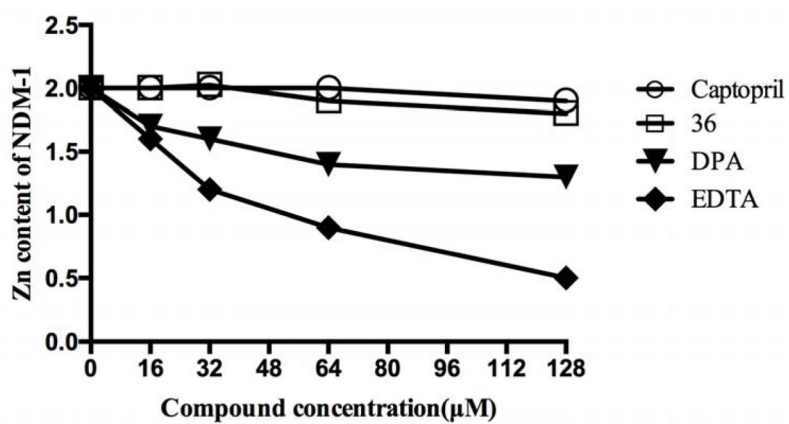


Figure 6. Metal content of NDM-1 (8 μM) after dialysis with various concentrations of EDTA, L-captopril, DPA, and **36** in 50 mM HEPES, pH 7.5 buffer.

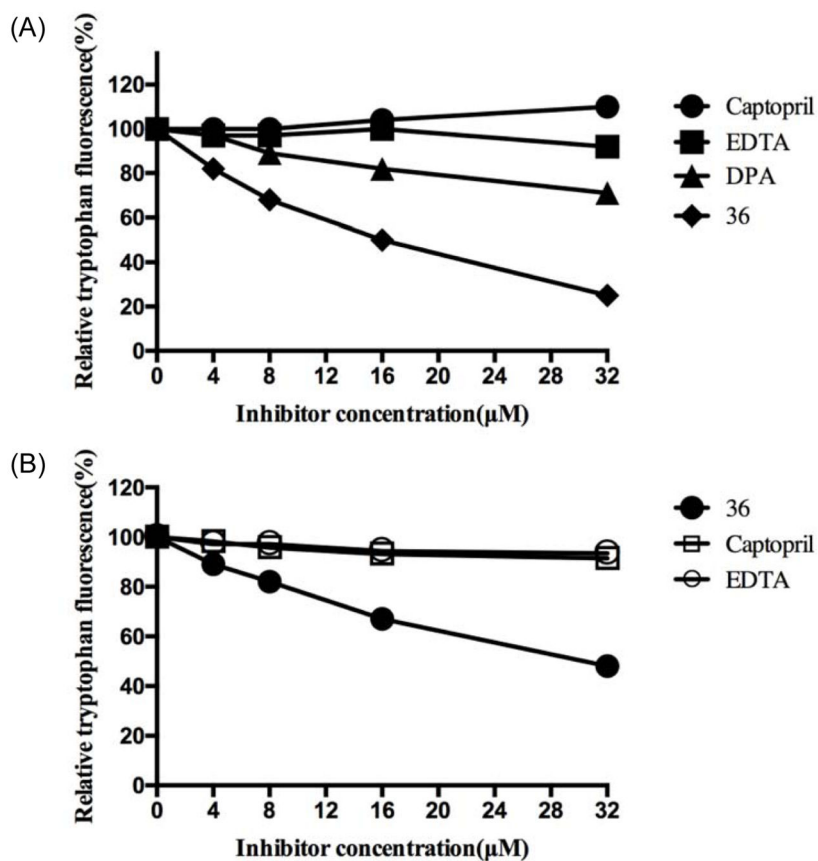
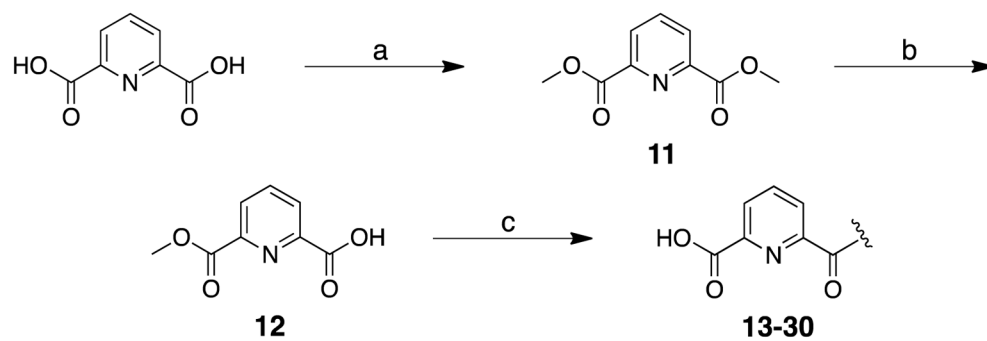
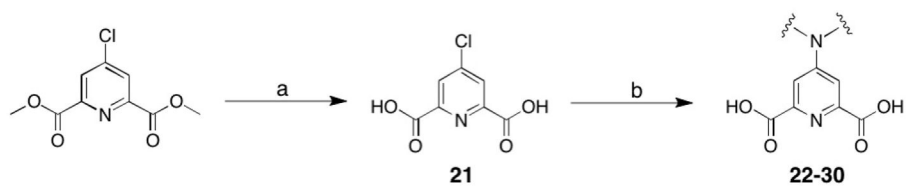


Figure 7. (A) Relative intrinsic tryptophan fluorescence emission versus concentration of inhibitor; (B) Relative intrinsic tryptophan fluorescence emission versus concentration of **36**, L-captopril and EDTA. The concentration of NDM-1 was 2 μM , L-tryptophan was 2 μM and the buffer for both studies was 50 mM HEPES, pH 7.5.

**Scheme 1.**

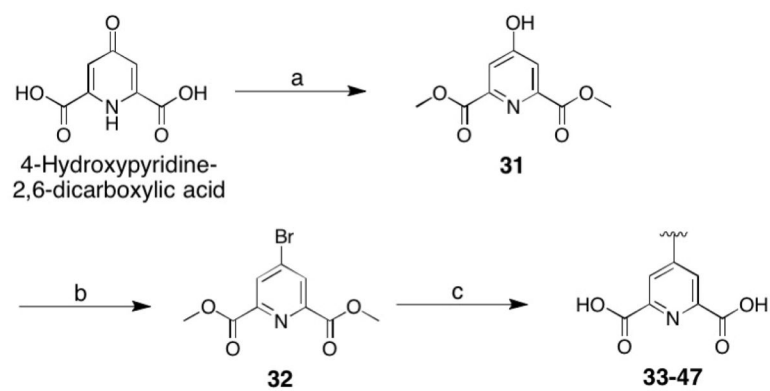
Synthetic scheme for sublibrary 1.

(a) MeOH, H₂SO₄ (cat.), 75 °C, 24 h, 100%; (b) MeOH, KOH, 0 °C, 4 h, 81%; (c) EDC, HOBT, H₂NR, 18 h; then 4:1 1 M NaOH:THF, 30 min – 1 h, 4 M HCl, 34–87%.

**Scheme 2.**

Synthetic scheme for sublibrary 2.

(a) 10:1 1 M NaOH:THF, 70 °C, 3 h, 80%; (b) amine, H₂O, microwave at 160 °C, 30 min, 10–80%.

**Scheme 3.**

Synthetic scheme for sublibrary 3.

(a) MeOH, H₂SO₄ (cat.), 75 °C, 24 h, 88%; (b) TBAB, P₄O₁₀, toluene, 100 °C, 3 h, 92%; (c) Pd(PPh₃)₄, K₃PO₄/CH₃CO₂K, 1,4-dioxane, 85 °C, overnight; then 4:1 1 M NaOH:THF, H₂SO₄, 22–84%.

Table 1

Examples of Select NDM-1 Inhibitors.

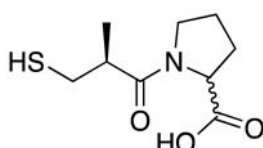
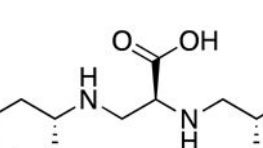
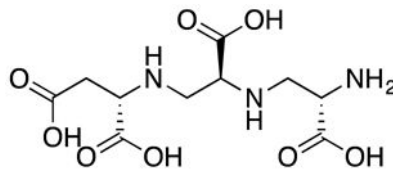
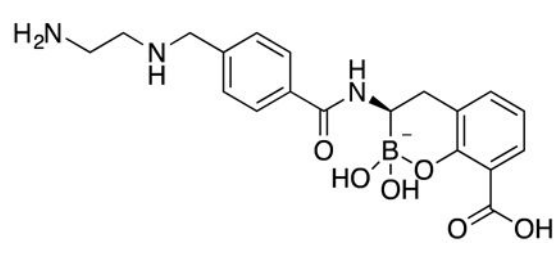
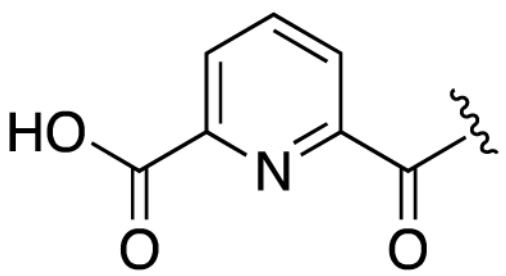
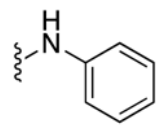
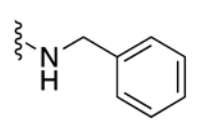
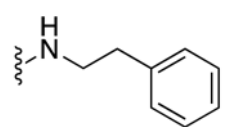
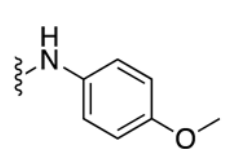
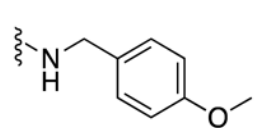
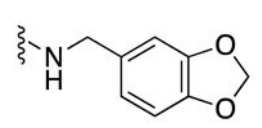
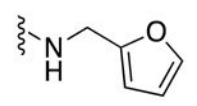
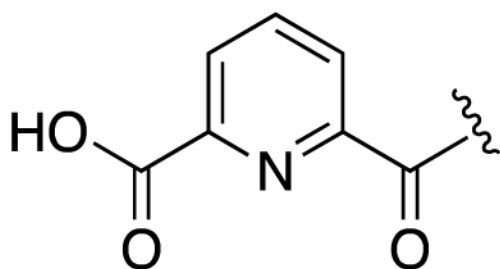
Structure	Name	IC ₅₀
	D-Captopril	7.9 μM^{14}
	L-Captopril	202.0 μM^{14}
	Aspergillomarasmine A (AMA)	4.0 μM^{12}
	Diamino-substituted cyclic boronate	4 nM ²⁰

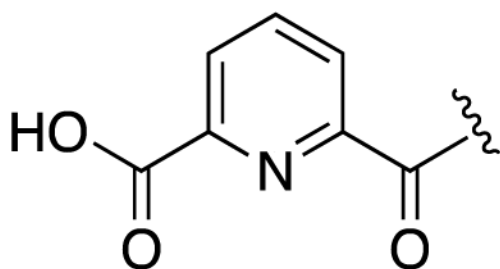
Table 2A

IC₅₀ Values of Sublibrary 1 Compounds (μM) Against NDM-1. Values were determined with chromacef at a substrate concentration of 3×K_M.

Number	Compound	IC ₅₀ (μM)
		
3		> 50
4		> 50
5		> 50
6		> 50
7		> 50
8		> 50
9		> 50



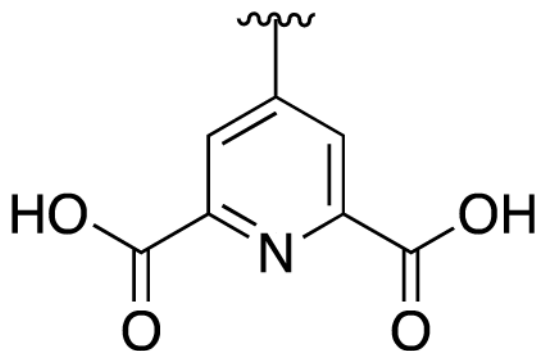
Number	Compound	IC ₅₀ (μM)
10		> 50
11		> 50
12		24 ± 1
13		49 ± 1
14		22 ± 1
15		> 50
16		> 50
17		> 50



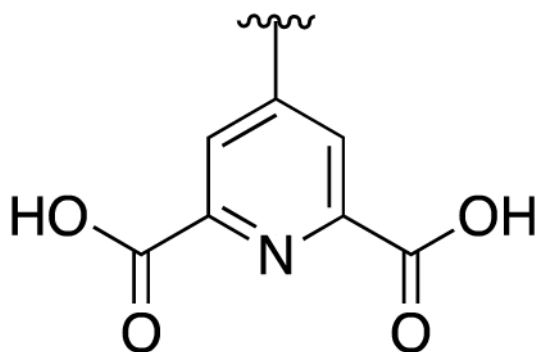
Number	Compound	IC ₅₀ (μM)
18	 <chem>*N1CCCCC1</chem>	> 50
19	 <chem>*N1CCOC1</chem>	> 50
20	 <chem>*N1CCCCC1</chem>	> 50

Table 2B

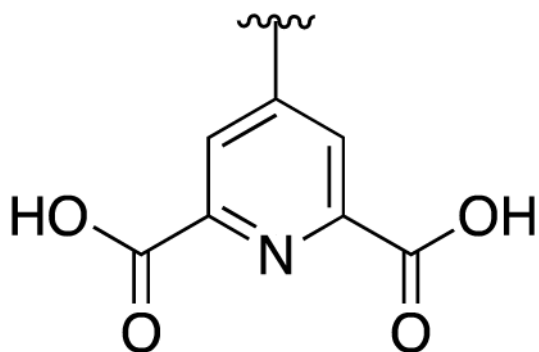
IC₅₀ Values of Sublibrary 2 and Sublibrary 3 Compounds (μM) Against NDM-1. Values were determined with chromacef at a substrate concentration of 3×K_M. Values in bold typeface were determined with fluorocillin at a substrate concentration <K_M.



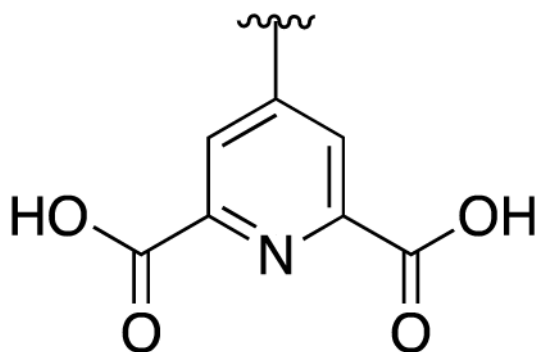
Number	Compound	IC ₅₀ (μM)
DPA	H	0.52 ± 0.04
		0.41 ± 0.02
21	Cl	5.0 ± 0.1
22		13.6 ± 0.8
23		3.4 ± 0.2
24		8.4 ± 1.1
25		9.1 ± 0.2
26		4.5 ± 0.1



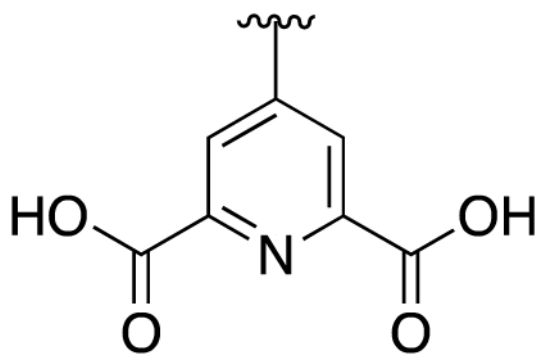
Number	Compound	IC ₅₀ (μM)
27		7.2 ± 0.4
28		5.8 ± 0.4
29		5.2 ± 0.1
30		4.9 ± 0.1
33		0.99 ± 0.02
34		0.80 ± 0.02 1.07 ± 0.07



Number	Compound	IC ₅₀ (μM)
		0.60 ± 0.03 0.43 ± 0.01
35		
		0.32 ± 0.01 0.08 ± 0.002
36		
		0.82 ± 0.01 0.43 ± 0.01
37		
		0.50 ± 0.02 0.50 ± 0.01
38		
		0.52 ± 0.02 0.13 ± 0.01
39		
		0.43 ± 0.02 0.38 ± 0.02
40		
		0.66 ± 0.03 0.39 ± 0.02
41		



Number	Compound	IC ₅₀ (μM)
42		1.03 ± 0.01
		0.54 ± 0.02
43		0.57 ± 0.02
		0.19 ± 0.01
44		0.89 ± 0.03
		0.20 ± 0.08
45		0.99 ± 0.04
		0.93 ± 0.02
46		0.86 ± 0.02
		0.13 ± 0.01



Number	Compound	IC ₅₀ (μM)
47	<p>Chemical structure of compound 47: a benzamide derivative with a wavy line substituent and a benzyl group.</p>	0.86 ± 0.02 0.59 ± 0.06

Table 3IC₅₀ Values of Selected Compounds with B1 MBLs Using Fluorocillin as a Substrate.

Compound	IC ₅₀ (μM)		
	NDM-1	VIM-2	IMP-1
DPA	0.41 ± 0.02	1.66 ± 0.03	3.03 ± 0.04
36	0.080 ± 0.002	0.21 ± 0.01	0.24 ± 0.01

Author Manuscript

Author Manuscript

Author Manuscript

Author Manuscript

Author Manuscript

Author Manuscript

Author Manuscript

Author Manuscript

Table 4Percent Inhibition of **36** (at 10 μ M) Against a Panel of Zn(II) Metalloenzymes.

	MMP-2	MMP-12	HDAC-1	HDAC-6	hCAII
36	<6%	48 \pm 8%	No inhibition	No inhibition	No inhibition

Table 5Microdilution Broth MICs of Clinical *E. coli* Isolates Expressing *bla*_{NDM-1}.

<i>E. coli</i> Isolates	MICs (mg/L)	
	Imipenem	Imipenem + 36
Ch8.68	16	1
Ch8.69	4	0.5
Ch8.70	16	0.5
Ah8.71	16	1
Ch8.72	16	0.5
Ah8.73	16	0.5
Ah8.74	8	0.5
Ah8.75	16	0.5

* All strains possess *bla*_{CTX-M-15} and *bla*_{CMY-2} except for *E. coli* Ah8.74 which possesses only *bla*_{NDM-1}.

Table 6Microdilution Broth MICs of Clinical *K. pneumoniae* Isolates Expressing *bla*_{NDM-1}.

<i>K. pneumoniae</i> Isolates	MICs (mg/L)	
	Imipenem	Imipenem + 3 β
Pd1.48	8	0.5
Pd1.49	4	1
Pd1.50	8	0.5
Pd1.53	8	0.5
Pd1.54	8	0.5
Pd1.55	8	0.5
Cm1.62	16	1
Cm1.63	8	1

* Strains Cm1.62 and Cm1.63 possess *bla*_{CTX-M-15} and *bla*_{CMY-2}. Strain Pd1.48 possesses *bla*_{SHV-12} and *bla*_{CTX-M-15}. Strains Pd1.49, Pd1.50, Pd1.53, Pd1.54, and Pd1.55 possess *bla*_{CTX-M-15}.